'Youth in Action' Programme
ERASMUS +

==========

TECHNICAL UNIVERSITY - SOFIA
English Language Faculty of Engineering

RESEARCH PROJECT

MEng Degree

An Investigation of the Dynamics of the Horizontal Wind Turbine Blades

Author: Itziar Urieta Nieto

Supervisor: eng. Cvetelina Velkova, PhD

Academic Year 2014 – 2015
Sofia, Bulgaria

==========

Contents

Acknowledgments

This research was supported by the English Language Faculty of Engineering at Technical University of Sofia (TU), in Bulgaria.

First of all, I would like to express my sincere gratitude to my main supervisor, Professor Cvetelina Velkova, who provided insight and expertise that greatly assisted the research. Thanks for giving me the opportunity to research on this interesting field, and for being supportive and patient through all the process.

I would also like to thank the Vice Rector, Professor Ivan Kralov for his help to find a subject that really interested me, his time and good advices during my time in the TU.

I wish to thank my coordinator, Professor Vladislav Slavov and the English Language Faculty of Engineering Dean, Tasho Tashev, for helping me in the first phase of my thesis and also everyday with the paperwork. Besides, I am very grateful for giving me the opportunity of discover new places in this country because of the trips that they organized.

Furthermore, I would also like to acknowledge the opportunity provided by the Public University of Navarre and the Erasmus Program, which made it possible to do my Master's Thesis at Technical University of Sofia.

Finally, special recognition goes out to my family, for their support, encouragement and patience during the whole degree and especially, during the preparation of this thesis. They are the pillar that holds my life and I could not have finished my university studies without them. Thanks also to my friends, who provided encouragement and allowed me to take time off from my duties for a while when I needed.

My entirely gratefulness.

List of Figures

List of Tables

List of Symbols

Note: This list is not exhaustive, and omits many symbols that are unique to particular chapters.

a	axial flow induction factor
a'	tangencial flow induction factor
A, A_D	rotor swept area
A_∞, A_w	upstream and downstream stream-tube cross-sectional areas
b	
B	number of blades
c	blade chord; Weibull scale parameter
C_D	sectional drag coefficient
C_L	sectional lift coefficient
C_p	power coefficient
D	drag force, rotor diameter
E	energy capture
F	force
F_{ax}	axial force
F_{tan}	tangencial force
$F()$	cumulative probability distribution
g	acceleration due to gravity
h	height
k	shape parameter for Weibull function
L	lift force
$\dot{m}$	mass flow
M	moment
Q	rotor torque
r	radius of the blade element o point on blade
R	resultant force
Re	Reynold's number
T	rotor thrust
u, U	wind velocity in x-direction
U_∞	free stream velocity
U_D	streamwise velocity at the rotor disc
U_w	streamwise velocity in the far wake

v, V	wind velocity in y-direction
w, W	wind velocity

Greek

α	angle of attack
β	pitch angle
λ	tip-speed ratio
μ	fluid viscosity
ν	kinematic viscosity
θ	angle of inclination
ρ	air density
ω	angular frequency (rad/s)
Ω	rotational speed of the rotor

Aim of the Project

The aim of this project is to design, investigate and model the aerodynamic behavior and dynamics of a wind turbine blades taking into account the elasticity of the rotor blades and the steadiness of the flow.

The main idea of the project is by performing the steady-state FSI (Fluid-Structure Interaction) analysis based on the obtained numerical results from two solvers: aerodynamic model for fluid and structural solver to evaluate the influence of the profile of wind turbine blade and position of the blades on the energy harvesting efficiency of a horizontal axis wind turbine blades (HAWT). The solution is obtained iteratively.

It should be resolved the following objectives so that to be satisfied the aim of this project:

- Developing of suitable aerodynamic model considering the deformation of aerodynamic loading for wind turbine blades.
- Developing the structural solver for determination of stresses and deformations on the wind turbine blades.
- Performing the steady-state FSI (Fluid-Structure Interaction) analysis of the obtained numerical results.
- Verification of the conducted numerical investigation is been performed by comparison of obtained numerical results for wind turbine blade tip velocity and wind turbine blade's radial force with analytical data calculated by using the simplified 1D momentum theory.

Chapter 1

Introduction

1.1. Energy Overview

Nowadays, people current living standard could not be maintained without energy and this need is increasing faster due to for example growing population, mobility, information and new technology. The main source of energy used is fossil fuels, which it involves coal, natural gas and oil. Humans have been using them since the start of the industrial revolution but this primary energy may runs out soon. Actually, energy demand rises almost every day and the reserves of fossil fuels are daily lower. This situation causes changes in the international price of the oil and as a result, economic and politic instability.

Besides, the provision of energy affects seriously to the environment so potential risks of global warming effect is only one example. Before the industrial revolution, concentration of CO_2 in the atmosphere was around 280 ppm but at present it is 380 ppm and it is rising every year due to gas emissions from burning fossil fuels, [1]. Combustion of primary energy also generates acids which fall to the Earth as acid rain, impacting in natural areas and buildings. These environment impacts are increasingly less tolerated by the current society, as well as by the energy and environmental policies of Europe.

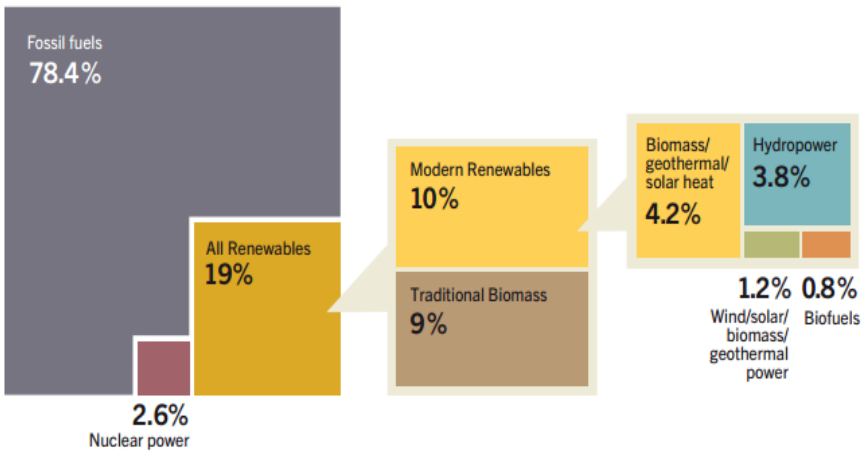

Figure 1.1: Estimated renewable energy share of global final energy consumption, 2012, [2]

In this point, renewable energy comes into picture, in order to determinate the economic and environmental viability of energy sources in the future. It is growing strongly and in 2012 supplied an estimated 19% of global final energy consumption, where 10% came from hydropower, wind, solar, geothermal, biofuels and modern biomass. Fuels can be substituted for them in areas such as power generation, cooling and heating and transport, [2]. See Figure 1.1 which showed explained above.

Furthermore, they have been aided by innovation and continuing advances of technology so the price of this energy has declined meanwhile the capacity has grown in a short period of time.

1.2. Wind Power

Usually, energy technologies take around 25 years to move from the research and development to commercial applications. However, wind technology had grown to the commercial stage in barely 10 years, beginning in the mid-70s. Their development took much less time due to, among other factors, the government incentives.

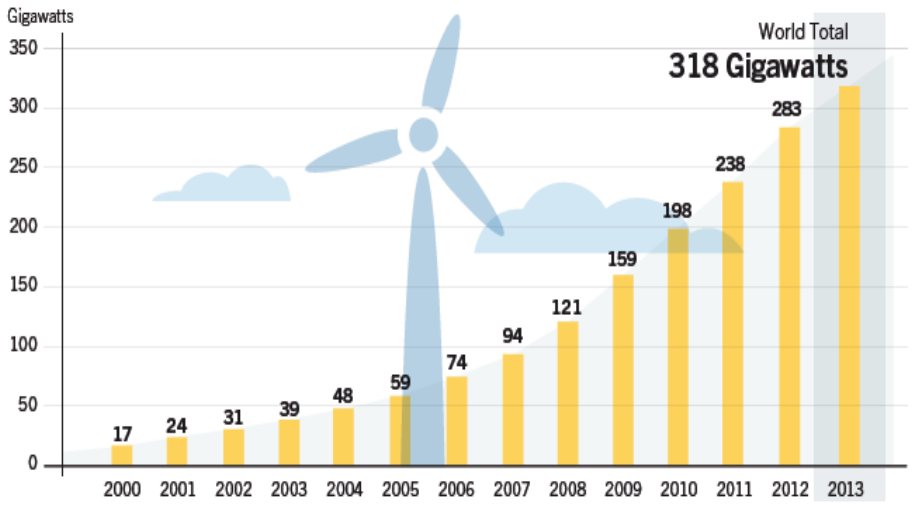

Figure 1.2: Wind Power Total World Capacity, 2000–2013, [2]

Nowadays, an estimated 35 GW of wind power capacity was put into operation during 2013, increasing global wind capacity above 318 GW, as it is shown in the Figure 1.2. The top ten countries for wind power capacity are China, United States, Germany, Spain, India, United Kingdom, Italy, France, Canada and Denmark; meanwhile the top wind turbine manufacturers are the following companies written in the Figure 1.3.

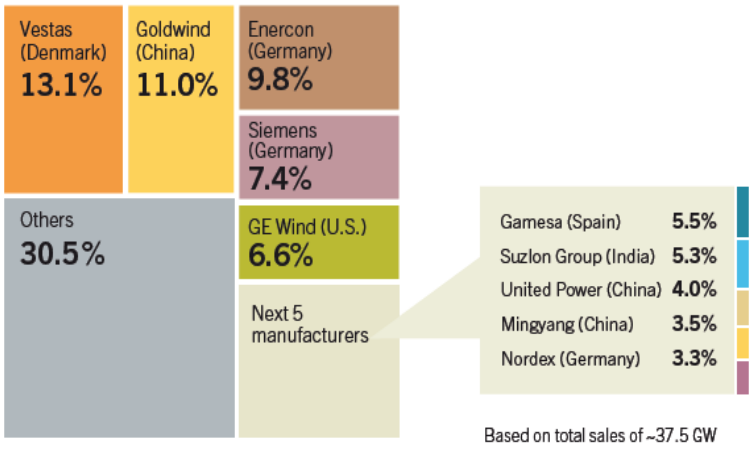

Figure 1.3: Market Shares of Top 10 Wind Turbine Manufacturers, 2013, [2]

The cost concerned wind turbines has declined dramatically over the years due to the increasing knowledge and development engineering of this technology promoted by the competition among manufacturers. The major reasons for these reductions in cost are associated with the growth in size of turbines, the cost of raw materials needed, improvements in manufacturing and installation techniques and the increased complexity of the systems. As a result, the cost of electricity from wind power has fallen measurably, too. In this way, it is achieved cost competitiveness relative to fossil fuels. Actually, onshore wind-generated KWh is now cost competitive in some markets. The number of projects of offshore technology has increased but also the cots because it has reached greater depths and distance from shore.

Figure 1.4 below describes the different cost of building a wind turbine. The most expensive parts are the tower, rotor blades and the gearbox which they add more than 50% of the total cost. In the case of the tower, it depends on the length as well as the material used (generally it is made of steel). Blades have increased in size over the years which it means a rise of prices. Finally, gearboxes need high cost of maintenance. In the future, they will be eliminated and replace it. Researches try to reduce the weight and complexity at the same time they look for increase the efficiency of the turbines.

Wind power has negative environmental and social impacts related with visual and aesthetic obstruction, noise generation, land-use impacts, wildlife mortality such as birds or bats, and consumption of raw materials. Some of them can be mitigated through technological innovation. An example is build turbine blades with thinner trailing edges in order to improve the efficiency and to generate less noise.

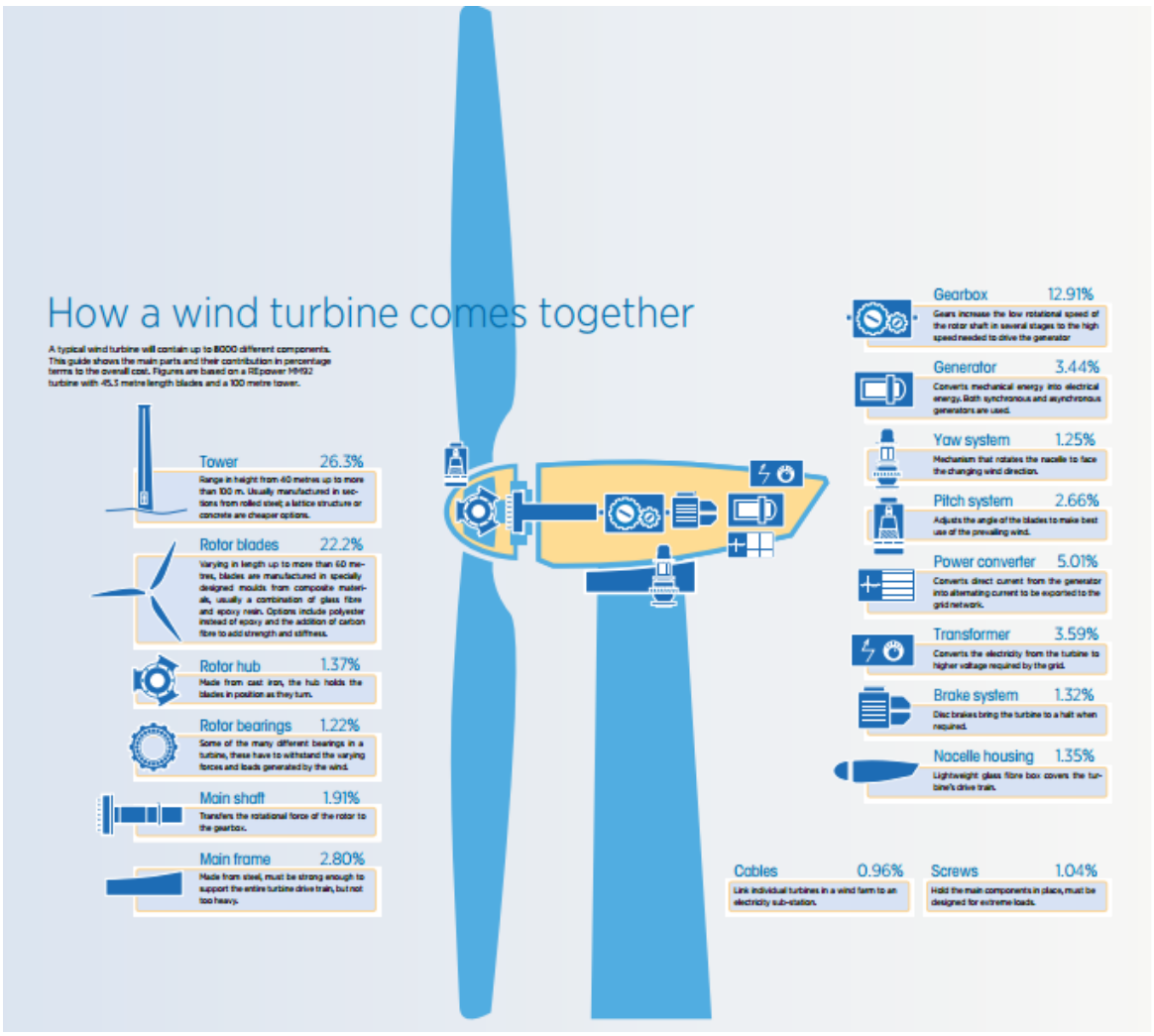

Figure 1.4: Parts and cost of a wind turbine, [3]

Chapter 2

Wind Turbine Classification

2.1. Introduction

Historically, wind power is one of the most ancient energy sources used by humans. Cultures such as Egyptians harnessed the force of the wind to propel boats along the Nile River around 5,000 B.C. as well as Persians pumped water and grinded grain using windmills between 500 and 900 B.C. Some years later, around 1,000 A.D. in The Netherlands, they were used to help drain lakes. Windmills convert wind power into rotational energy through the blades which are connected to a hub, [4]. The result of the development of mills over the time in order to produce electrical energy leads to the appearance of wind turbines. Examples of wind turbines and windmills are represented in Figure 2.1.

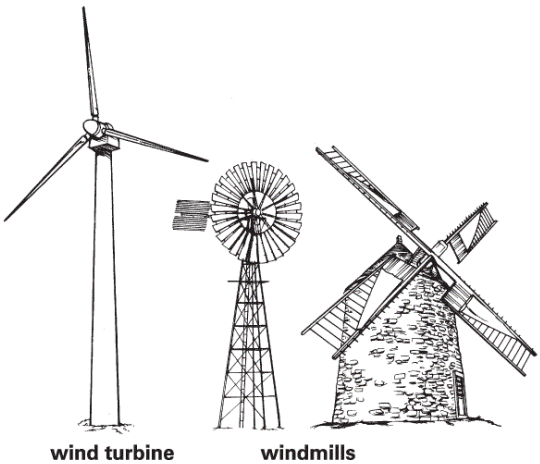

Figure 2.1: Wind Turbine and Windmills, [5]

Broadly, wind turbine are classified in two categories considering the orientation of the axis of rotation. On the one hand are Horizontal Axis of Wind Turbines (HAWT) and on the other hand are Vertical Axis of Wind Turbines (VAWT). The first one are used more often, because of that, they were chosen in this project.

2.2. VAWT

Vertical Axis of Wind Turbine have the main rotor situated vertically, allowing the location of the heavy components such as the gearbox and the generator close to the ground and hence easily accessible in order to improve the maintenance. Even this arrangement allows the lack of the tower which is an advantage in relation to the cost but a disadvantage considering the energy achieved because the speed of the wind near the ground is lower due to it increases air friction with the ground.

This kind of wind turbine is capable of catching the wind from all directions so that they do not require yaw mechanism. However, some designs are not self-starting and they need guy wires to hold them.

There are two well-known types of VAWT:

2.2.1. Rotor Darrieus

The first one was developed by George Darrieus in France in 1927 and it consists of two blades or more disposed as the Figure 2.2 (above). It is based on the principle of the lift whose force propels the turbine moving the blades in a rotational way. Their efficiency can be compared to HAWT but it needs additional guy wires to ensure the stability.

2.2.2. Rotor Savonious

The Savonious turbine was introduced by S.J. Savonious in Finland in 1922 and it is distinguished by having two half-cylinder blades which are cut by a generatrix and laterally displaced. This kind of rotor operates using drag forces. It can be integrated into buildings but due to their low efficiency, they are barely used.

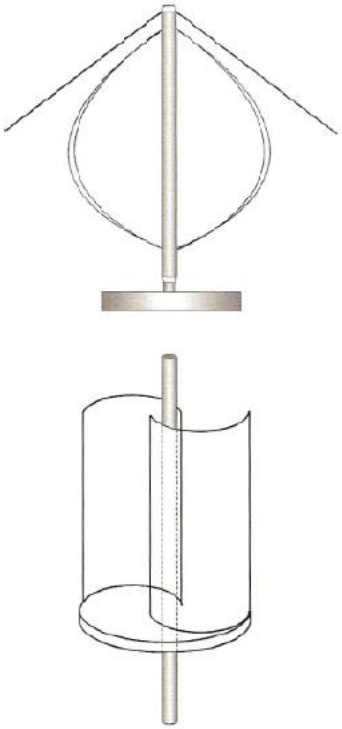

Figure 2.2: VAWT (Darrieus above and Savonious below), [6]

2.3. HAWT

The blades' rotation of Horizontal Axis of Wind Turbines is perpendicular to the direction of the incident wind speed. The influence of a few characteristics on the aerodynamics of HAWT are described below.

2.3.1. Number of blades

The number of blades is directly related with the aerodynamic efficiency so as the number of blades in the wind turbine increases, the energy absorbed would be higher. This affirmation might suggests that an infinite number of blades will convert the whole energy from the wind; however, the efficiency gain increases in a diminishing manner and it has also a maximum value given by the Betz limit. A more efficiency turbine is obtained when it has slow turning and few blades (1, 2 or 3).

Hence, when a 2-blade turbine is replaced to a 3-blade one, the efficiency gain is about 3%, whereas changing a 3-blade design to a 4-blade the gain is marginal, [4]. This concept is described in Figure 2.3.

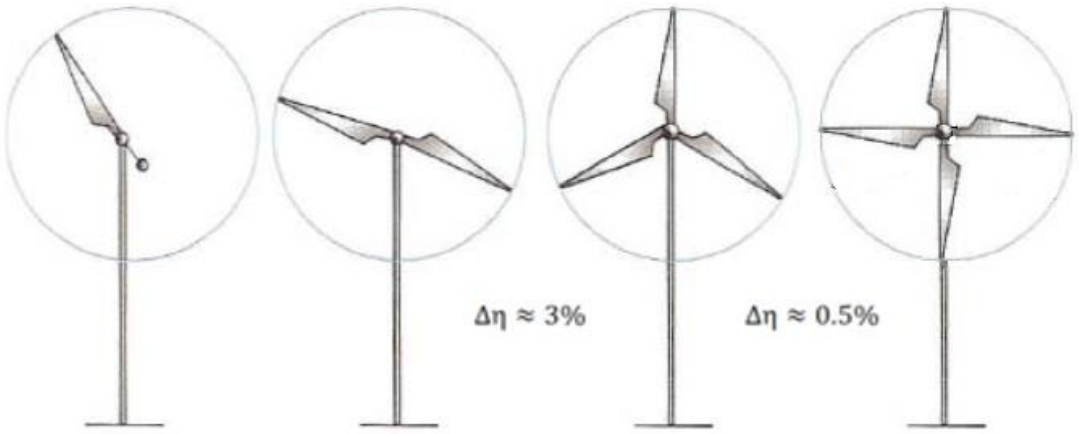

Figure 2.3: Efficiency gain as number of blades in wind turbine is increased

'¿Why is the 3-blade wind turbine chosen as the most common?' In order to find a balance between the drag force and the torque. As a consequence of an increased number of blades, drag increases too, so that a bigger pole is needed because the wind turbine could fall down.

Describing below the advantages and disadvantages from the different types of rotors compared to the three-blade one, which they are 120 degrees among them. In the case of a wind turbine with only one blade, this design requires a counterweight at the other end to balance the rotor.

The rotor has to be able to lean to avoid strong shaking each time the blade passes near the tower. Besides, it needs a higher rotational speed in order to produce the same the energy, implying more noise. However, it saves the cost of two blades and the weight of them, [7]. As the number of blades increased, the cost of the system increases drastically and the blades should be thinner to be aerodynamically efficient, [5].

Figure 2.4 describes the power coefficients (C_p) of various types of wind turbine rotor versus tip-speed ratio (λ). These concepts are explained in the following chapter.

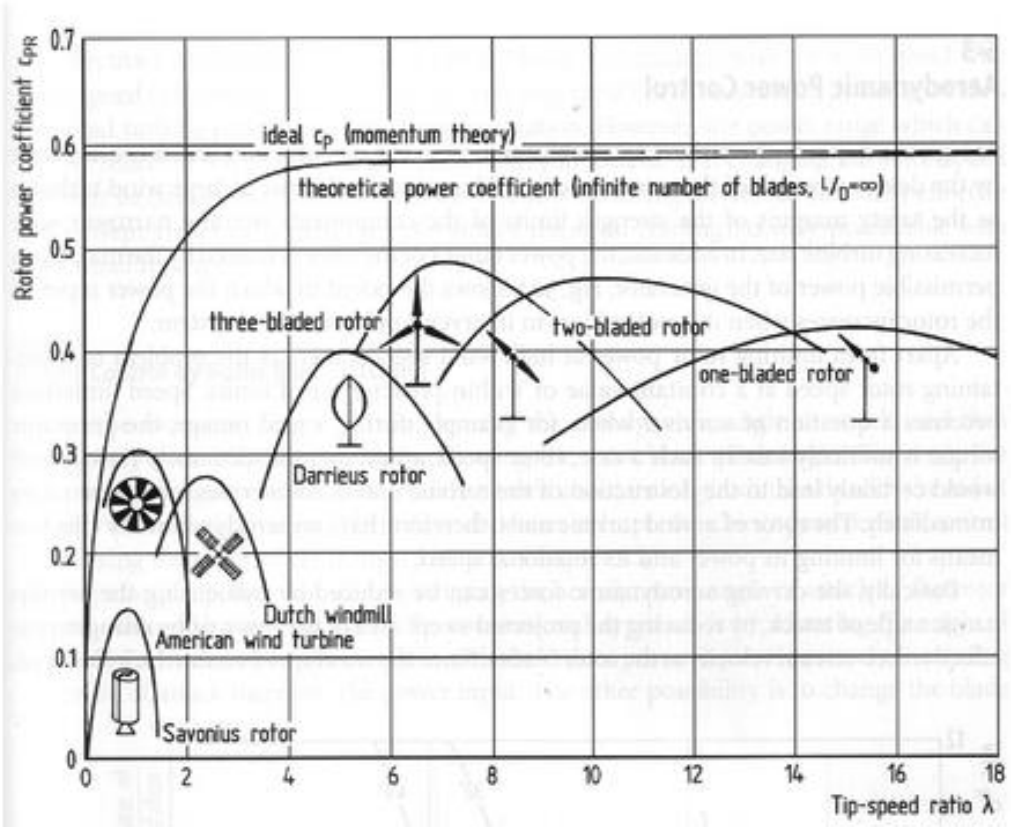

Figure 2.4: The power coefficients (C_p) of various types of wind turbine rotor plotted versus tip-speed ratio (λ), [8]

2.3.2. Blades orientation

There are two types: upwind and downwind turbines.

- **Upwind Turbines:**

The shaft of the rotor and generator in upwind turbines are positioned horizontally and the wind hits blades before the tower, implying that the rotor is facing the wind. The wind shade behind the tower is avoided and it deviates from it before reaching. Because of that, there is a little loss of power whenever the rotor passes the tower.

The main disadvantage of this design is the problem related with the bending back into the tower due to the striking of blade, so that, it is required to position the rotor far enough away from the tower. It needs a yaw mechanism in order to maintain the position of the rotor and an inflexible rotor.

'¿How to get flexibility in the rotor?' Two different solves are describing below. The first one is the cone angle (0-3 degrees) which it provides certain angle to the rotor that allows to separate the blades from the tower while tilt angle (0-3 degrees) is the angle between the horizontal axis and the rotor shaft. The last one gives the machine some inclination, (see Figure 2.5).

- **Downwind Turbines:**

In this case, the wind has to pass through the tower before striking the blades. The rotor can be flexible due to there is no danger of a tower strike. However, there are fluctuations caused by the tower shade.

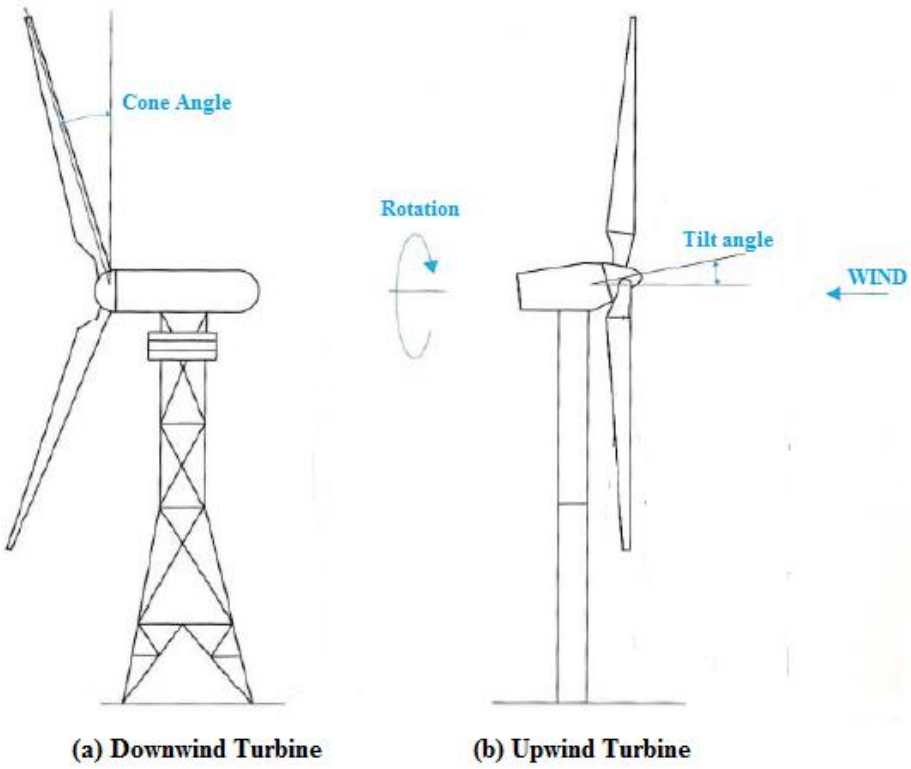

Figure 2.5: (a) Downwind turbine and (b) Upwind turbine

Chapter 3

Theoretical Formulation of the Problem

3.1. Introduction

This chapter sets out the basis of the aerodynamics of HAWTs and also describes the main analyses of the aerodynamic behavior in steady wind conditions without any specific turbine design, just by considering the energy extraction process. Accordingly, some knowledge of fluid and aircraft dynamics are required before, in order to understand it.

3.2. The Wind Resource

The energy available in the wind varies as the cube of the wind speed, so an understanding of the characteristics of the wind resource is critical to all aspects of wind energy exploitation, from the identification of suitable sites to the design of wind turbines. From the point of view of wind energy, the most striking characteristic of the wind resource is its variability. The wind is highly variable, both geographically and temporally, [9].

$$P_{wind} = \frac{1}{2}\rho A u^3 \tag{3.1}$$

The Earth's surface has irregularities and inequalities of heating, consequently of these features, the wind flow is also modified. Figure 3.1 shows that the wind varies geographically and Figure 3.2 is an example of the three types of terrains which describes that the wind speed increases with altitude due to the reduction of the friction. According with that, an exponential variation in wind speed with height is defined.

$$u_{top} = u_{point\ of\ measured}\left(\frac{h_{top}}{h_{point\ of\ measured}}\right)^{\alpha_{Hellman}} \tag{3.2}$$

The parameter $\alpha_{Hellman}$ is called Hellman's exponent and it varies according to the rugosity of the terrain. In the case of a wind turbine, the $h_{point\ of\ measured}$ will be the low of the blade.

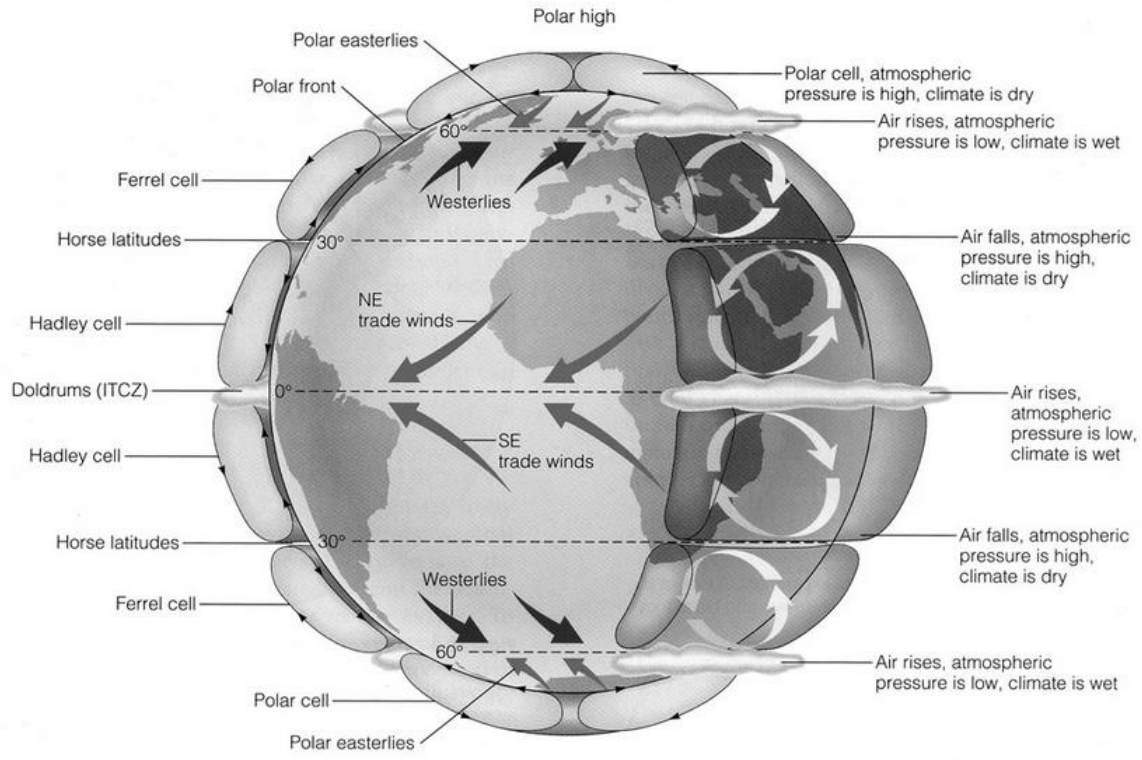

Figure 3.1: Global air circulation, [10]

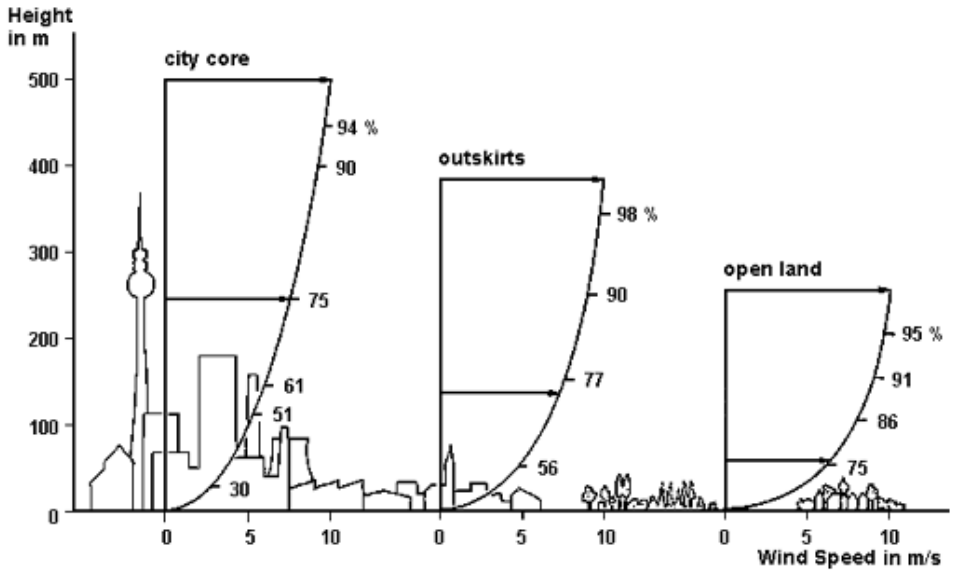

Figure 3.2: Wind profile depending of the type of terrain, [11]

The wind speed varies also according to the time, during the year because of seasonal changes and also along the day.

All these changes add significantly to the uncertainty in predicting the energy output. However, variations during the year can be well characterized in terms of a probability distribution. The Weibull distribution provides a reasonably good representation of the variation wind in relation of the annual hours, [9]. This distribution takes the form

$$F(U) = exp\left(-\left(\frac{U}{c}\right)^{k}\right) \tag{3.3}$$

where $F(U)$ is the fraction of time for which the hourly mean wind speed exceeds U. It is characterized by two parameters: a 'scale parameter' c and a 'shape parameter' k. An example of Weibull distributions is represented in the Figure 3.3.

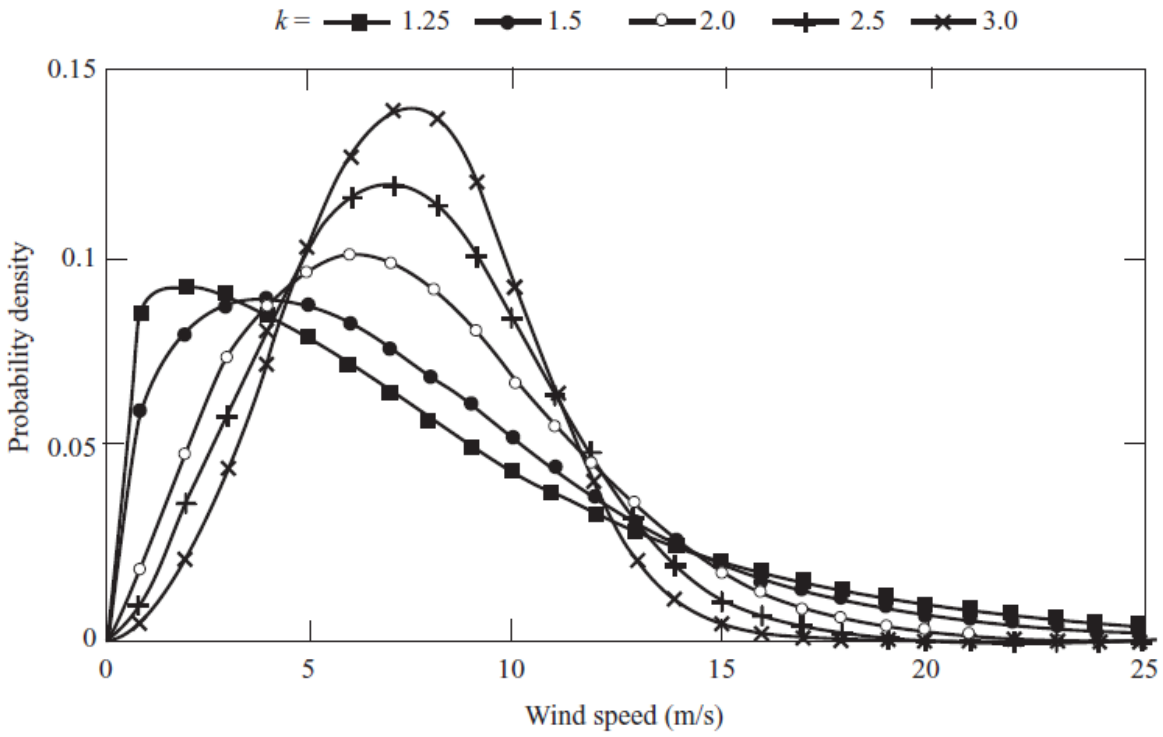

Figure 3.3: Example Weibull distributions, [9]

3.3. Betz Law

Wind turbines extract energy by slowing down the wind, so that the speed of the wind before reaching the blade is higher and when it passes through the blade, braking occurs while allowing a continuation of the flow. However, wind turbines cannot extract all the kinetic energy from the wind since according to the theory established by the German engineer Betz, there is a limit in the quantity of energy absorbed. This limit is defined by a parameter denoted as the power coefficient C_p, which maximum value is 0.593.

Betz limit indicates the maximum energy absorbed and therefore, the maximum value of the efficiency of a turbine which cannot exceed 59.3% efficiency, as noted above. Betz equation deals with the wind speed upstream of the turbine U_∞ and the downstream wind speed U_w. To develop the equation, it is necessary to make some assumptions and to choose a control volume, which are specified below and represented in Figure 3.4.

- It is considered an ideal rotor, meaning that:
  1. It does not possess a hub.
  2. It has got an infinite number of blades.
  3. The value of the drag resistance is zero, implying that the thickness is also zero.

- The wind speed must slow down but only the mass of air which pass through the rotor is affected. Besides, it is also considered uniform and it is denoted as U_D. In this way, the control volume is forming by a long stream-tube of circular cross section where U_∞ is the upstream speed and U_w is downstream wind speed.
  Therefore $U_\infty > U_w$.

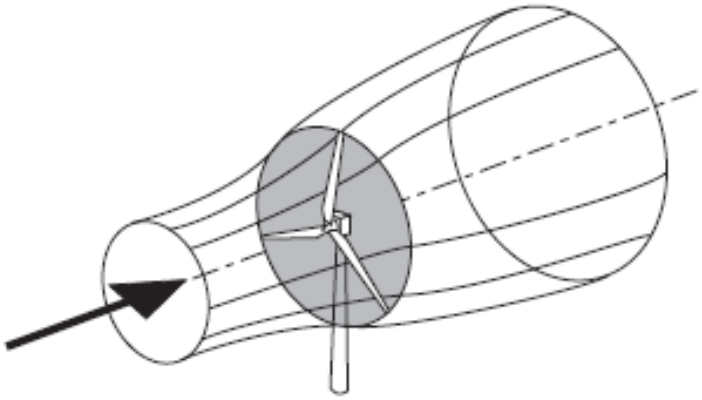

Figure 3.4: Stream-tube chosen as a control volume, [9]

- The flow into and out of the rotor is assumed to be axial. Swept area beyond the control volume is uniform. The air cross sectional area swept upwind is designated as A_∞, and downwind as A_w whereas the cross-section blade is A_d.
  As a result $A_w > A_\infty$.

- It is incompressible flow (density remains constant) and there is no heat transfer between the rotor and the flow, [7].

- The ideal model is shown in the Figure 3.5.

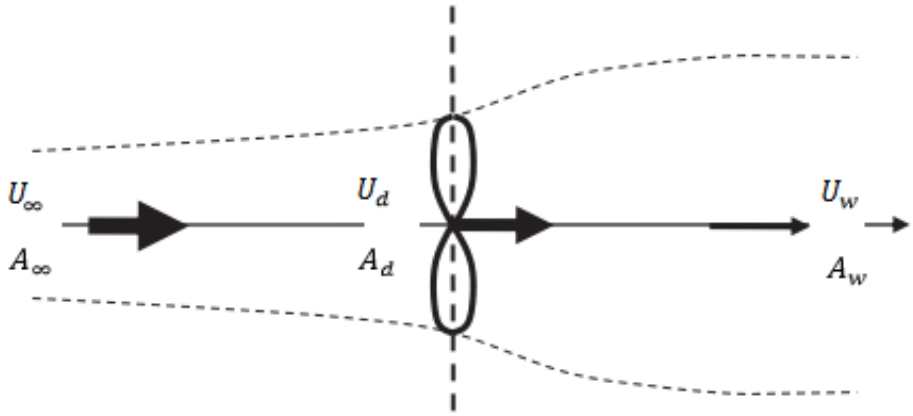

Figure 3.5: Ideal model used in Betz law, [12]

Applying the equation of conservation of mass, the same volume of fluid must flow in both sections A_∞ and A_w in a given time interval, which implies that

$$\dot{m} = \rho A_\infty U_\infty = \rho A_D U_D = \rho A_w U_w \tag{3.4}$$

Power of the rotor is represented by the equation (3.6) given below,

$$F = m \cdot a = m\frac{dU}{dt} = \dot{m} \cdot \Delta U = \dot{m}(U_\infty - U_w) = \rho A_D U_D (U_\infty - U_w) \tag{3.5}$$

$$dE = F \cdot dx \quad \Rightarrow \quad P = \frac{dE}{dt} = F\frac{dx}{dt} = \rho A_D {U_D}^2 (U_\infty - U_w) \tag{3.6}$$

Power of the wind is related to kinetic energy, as well

$$P_{wind} = \frac{\mathrm{d}E}{\mathrm{d}t} = \frac{d\left(\frac{1}{2}m \cdot \Delta U^2\right)}{dt} = \frac{1}{2}\dot{m}\left({U_\infty}^2 - {U_w}^2\right) = \frac{1}{2}\rho A_D U_D \left({U_\infty}^2 - {U_w}^2\right) \tag{3.7}$$

Equating the two equations of the power given in (3.6) y (3.7), in order to obtain the wind velocity at the rotor

$$P = \frac{1}{2}\rho A_D U_D \left({U_\infty}^2 - {U_w}^2\right) = \rho A_D {U_D}^2 (U_\infty - U_w) \tag{3.8}$$

$$\frac{1}{2}\left({U_\infty}^2 - {U_w}^2\right) = \frac{1}{2}(U_\infty - U_w)(U_\infty + U_w) \tag{3.9}$$

$$\frac{1}{2}(U_\infty - U_w)(U_\infty + U_w) = U_D(U_\infty - U_w), \quad \forall\, \rho, U_D, A_D \neq 0 \tag{3.10}$$

$$U_D = \frac{1}{2}(U_\infty + U_w), \quad \forall\, (U_\infty - U_w) \neq 0, \; or\; U_\infty \neq U_w \tag{3.11}$$

The equation (3.11) shows that the wind velocity at the rotor could be taken as the average of the upstream and downstream wind velocities and besides, the flow must be maintained to extract energy from the wind stream. If the power is represented in terms of the upstream and downstream velocities, it might be obtained the maximum value of the extracted energy.

$$P = \frac{1}{2}\rho A_D U_D\left({U_\infty}^2 - {U_w}^2\right) = \frac{1}{2}\rho A_D \frac{1}{2}(U_\infty + U_w)\left({U_\infty}^2 - {U_w}^2\right) \tag{3.12}$$

Developing the equation (3.12),

$$\begin{aligned} P &= \frac{1}{4}\rho A_D\left({U_\infty}^3 + {U_\infty}^2 U_w - U_\infty {U_w}^2 - {U_w}^3\right) \\ &= \frac{1}{4}\rho A_D {U_\infty}^3\left(1 + \frac{U_w}{U_\infty} - \frac{{U_w}^2}{{U_\infty}^2} - \frac{{U_w}^3}{{U_\infty}^3}\right) \end{aligned} \tag{3.13}$$

A parameter b could be defined as the ratio between U_w and U_∞, it also can be introduced in the expression to obtain the maximum power,

$$\frac{dP(b)}{db} = \frac{dP\left(1+b-b^2-b^3\right)}{db} = 0 \quad \Rightarrow \quad b_{max} = \frac{U_w}{U_\infty}\Big|_{max} = \frac{1}{3} \tag{3.14}$$

As a result,

$$P_{max} = \frac{8}{27}\rho A_D {U_\infty}^3 = \frac{16}{27}\left(\frac{1}{2}\rho A_D {U_\infty}^3\right) \tag{3.15}$$

$$C_{p_{max}} = \frac{P_{max}}{P_{wind}} = \frac{\frac{16}{27}\left(\frac{1}{2}\rho A_D {U_\infty}^3\right)}{\frac{1}{2}\rho A_D {U_\infty}^3} = \frac{16}{27} \tag{3.16}$$

Figure 3.6 is represented below to describe the behavior of C_p versus the parameter b.

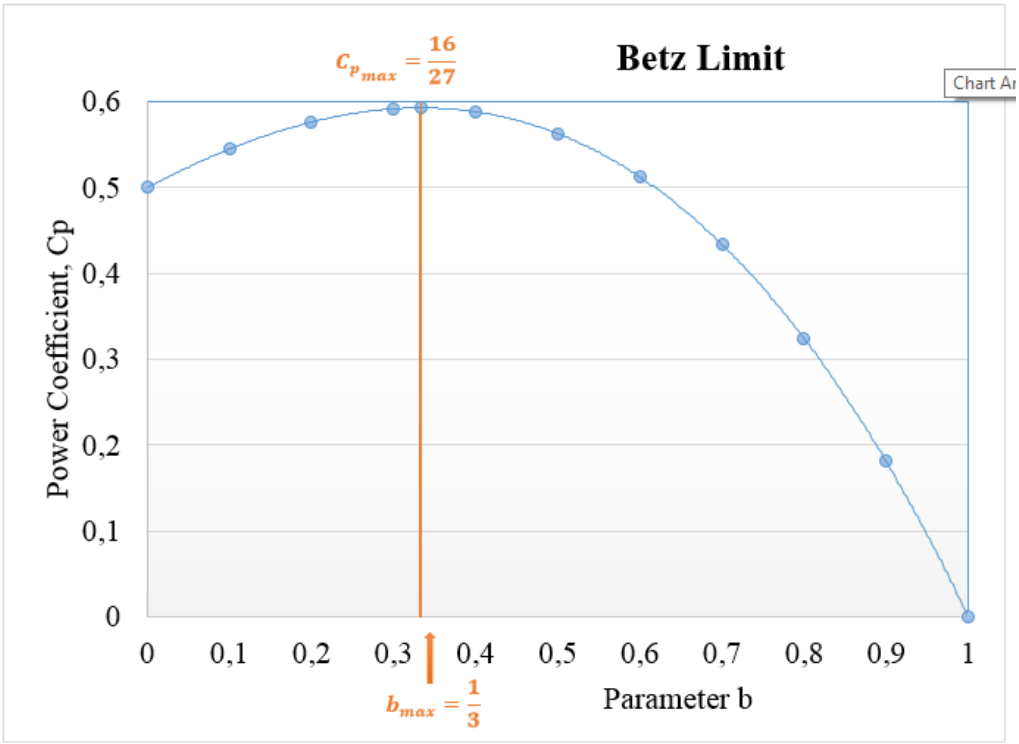

Figure 3.6: Betz limit

3.4. Actuator Disc Theory

This theory combines the momentum and mass conservation, as well as it takes into account the effects of a rotational wake.

3.4.1. Linear Momentum

A one-dimensional analysis of a wind turbine rotor, which is represented by an infinitesimal disc area A, is performed. It is moving through an incompressible, isentropic, no-rotational and inviscid fluid. Besides, frictional forces between fluid and disc are despised, and fluid velocity is considered uniform along parallel sections of the rotor.

Upstream of the disc the stream-tube has a cross-sectional area smaller than that of the disc and an area larger than the disc downstream. The expansion of the stream-tube is because the mass flow rate must be the same everywhere so the mass conservation could be established, [9]. Related the velocity and the pressure, the flow speed decreases slowly when it passes through the disc meanwhile the pressure undergoes a sharp decline. Thus, the stream-tube is well-defined as shown in the Figure 3.7.

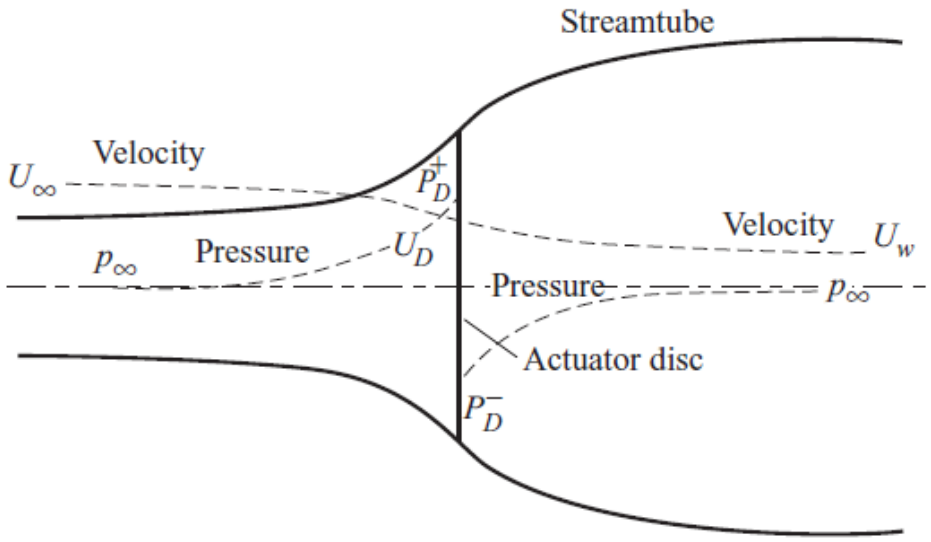

Figure 3.7: Concept of actuator disc theory and stream-tube, [9]

The mass of air which passes through a given cross-section of the stream-tube in a unit length of time is ρAU, where ρ is the air density, A is the cross-sectional area and U is the flow velocity. The symbol ∞ refers to conditions far upstream, D refers to conditions at the disc and w denotes to conditions in the far wake.

$$\dot{m} = \rho A_\infty U_\infty = \rho A_D U_D = \rho A_w U_w \tag{3.17}$$

The actuator disc induces a velocity variation which must be superimposed on the free stream velocity, where a is called inflow factor.

$$U_D = U_\infty(1 - a) \tag{3.18}$$

3.4.2. Simple Momentum Theory

There is a pressure difference across the actuator disc because the stream-tube is completely surrounded by air at atmospheric pressure, which gives zero net force. Therefore,

$$(p_D^+ - p_D^-)A_D = (U_\infty - U_w)\rho A_D U_\infty (1-a) \tag{3.19}$$

To obtain the pressure difference $(p_D^+ - p_D^-)$, Bernoulli's equation is applied separately to the upstream and downstream sections of the stream-tube because the total energy is different in each section. Assuming the flow to be incompressible $(\rho_\infty - \rho_D)$ and horizontal $(h_\infty - h_D)$ then,

Upstream,

$$\frac{1}{2}\rho U_\infty^2 + p_\infty = \frac{1}{2}\rho U_D^2 + p_D^+ \tag{3.20}$$

Similarly, downstream,

$$\frac{1}{2}\rho U_w^2 + p_\infty = \frac{1}{2}\rho U_D^2 + p_D^- \tag{3.21}$$

Subtracting these equations,

$$(p_D^+ - p_D^-) = \frac{1}{2}\rho(U_\infty^2 - U_w^2) \tag{3.22}$$

Equation 3.19 then gives,

$$\frac{1}{2}\rho A_D(U_\infty^2 - U_w^2) = (U_\infty - U_w)\rho A_D U_\infty (1-a) \tag{3.23}$$

and so,

$$U_w = (1-2a)U_\infty \tag{3.24}$$

That is, half the axial speed loss in the stream-tube takes place upstream of the actuator disc and half downstream, [9].

3.4.3. Power Coefficient

The force on the air, called also torque, becomes, from Equation 3.19

$$T = (p_D^+ - p_D^-)A_D = 2\rho A_D U_\infty^2 a(1-a) \tag{3.25}$$

This force is concentrated at the actuator disc and the work (power extraction form the air) done by the force is

$$P = TU_D = 2\rho A_D U_\infty^3 a(1-a)^2 \tag{3.26}$$

Thus, the power coefficient is defined as

$$C_p = \frac{P}{P_{wind}} = 4a(1-a)^2 \tag{3.27}$$

3.5. Rotor Disc Theory

The rotation of the wind turbine blades employs an angular velocity Ω about an axis normal to the rotor plane and parallel to the wind direction. The blades sweep out a disc and develop a pressure difference across the disc, which is responsible for the loss of axial momentum in the wake. As well as a thrust, the rotor experiences a torque in the direction of rotation that will oppose the torque that the generator exerts.

3.5.1. Wake Rotation

The exertion of a torque on the rotor disc by the air passing through it requires an equal and opposite torque to be imposed upon the air. The consequence of the reaction torque is to cause the air to rotate in a direction opposite to that of the rotor; the air gains angular momentum and so in the wake of the rotor disc the air particles have a velocity component in a direction which is tangential to the rotation as well as an axial component, [9].

Air rotates because of the forces momentum of the blades. The total rotation of the air is made by an induced rotation before the collision with the blades and the rotation after passing through the blades. Both rotations are considered equal as an approximation, (see Figure 3.8).

Thus, the air rotation at the entrance of the blades is $\Omega a'$ and at the output of the blades is $2\Omega a'$, both in the opposite direction of the blades rotation.

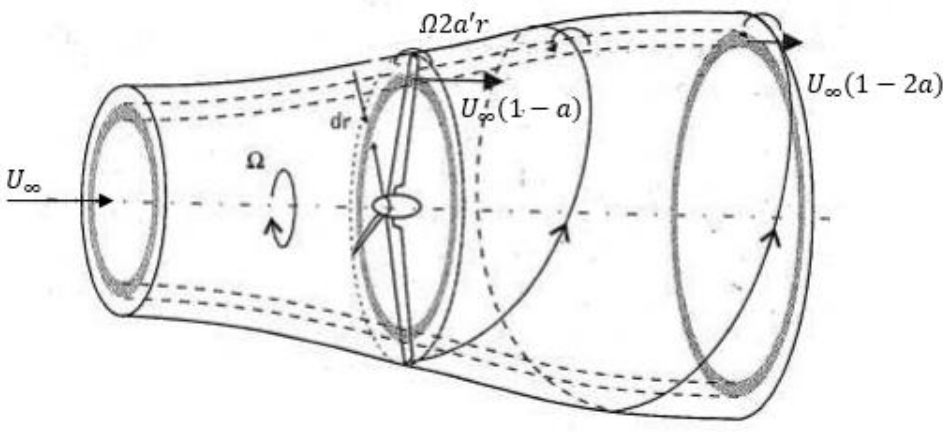

Figure 3.8: Concept of rotor disc theory

3.6. Blade Element Momentum (BEM) Theory

Aerodynamic forces (lift and drag) on the span-wise elements of radius r and length δr of the several blades of a wind turbine rotor are responsible for the rate of change of axial and angular momentum of all of the air which passes through the annulus swept by the blade elements. In addition, the force on the blade elements caused by the drop in pressure associated with the rotational velocity in the wake must also be provided by the aerodynamic lift and drag, [9].

3.6.1. Blade Element Theory

Blade element theory is a 2D analysis about the wind turbine blades, which takes into account the design and the number of blades in order to obtain the torque and the power. It is based on the actuator disc and rotor disc theories.

It is assumed that the forces on a blade element can be calculated by using an angle of attack. The velocity components of the wind speed, the flow factors and the rotational speed of the rotor determine the angle of attack. Having information about coefficients C_L and C_D, which vary with the angle of attack, the forces on the blades for given values of a and a' can be determined, (see Figure 3.9).

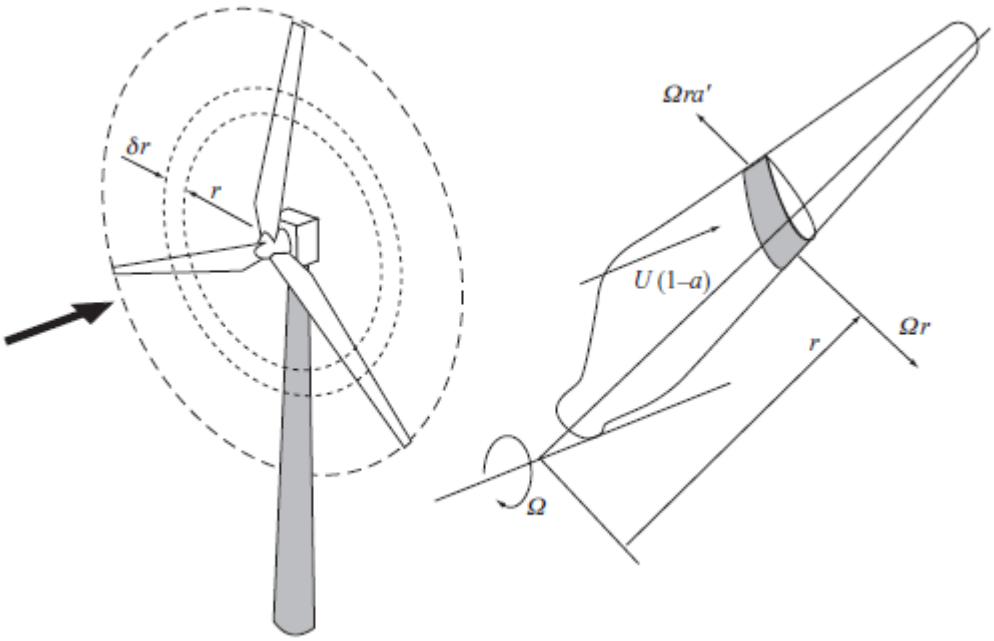

Figure 3.9: Blade element sweeps out an annular ring, [9]

Consider a turbine with B blades of tip radius R each, with chord c and set pitch angle β measured between the airfoil zero lift line and the plane of the disc. Both the chord length and the pitch angle may vary along the blade span. Let the blades be rotating at angular velocity Ω and let the wind speed be U_∞, [9].

Figure 3.10 shows all the velocities and forces relative to the blade chord line at radius r. From this picture the resultant relative velocity at the blade is

$$W = \sqrt{U_\infty^2(1-a)^2 + r^2\Omega^2(1+a')^2} \tag{3.28}$$

That acts at an angle ϕ to the plane of rotation such that

$$\sin\phi = \frac{U_\infty(1-a)}{W} \quad \text{and} \quad \cos\phi = \frac{r\Omega(1+a')}{W} \tag{3.29}$$

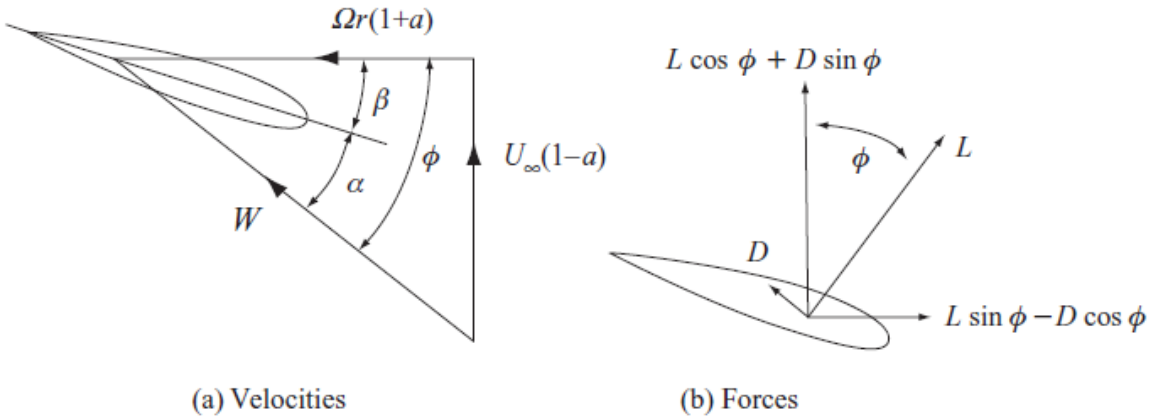

Figure 3.10: Blade element velocities and forces, [9]

The angle of attack α is then given by

$$\alpha = \varphi - \beta \tag{3.30}$$

Following the representation of the forces in Figure 3.10, the lift force (equation (3.31)) and the drag force (equation (3.32)) on a span-wise length δr of each blade are

$$\delta L = \frac{1}{2}\rho W^2 c C_L \delta r \tag{3.31}$$

$$\delta D = \frac{1}{2}\rho W^2 c C_D \delta r \tag{3.31}$$

The axial thrust (F_{ax}) on an annular ring of the actuator disc is

$$\delta T = \delta L\cos\phi + \delta D\ sen\ \phi = \frac{1}{2}\rho W^2 Bc(C_L\cos\phi + C_D sen\ \phi)\delta r \tag{3.32}$$

The tangential force (F_{tan}) on an annular ring of the actuator disc is

$$\delta F_{tan} = \frac{1}{2}\rho W^2 Bc(C_L\sin\phi + C_D cos\ \phi)\delta r \tag{3.33}$$

The torque on an annular ring is

$$\delta Q = r\,\delta F_{tan} = \frac{1}{2}\rho W^2 Bcr(C_L \sin\phi + C_D cos\,\phi)\delta r \tag{3.34}$$

The power on an annular ring is

$$\delta P = \Omega r\,\delta F_{tan} = \frac{1}{2}\rho W^2 Bcr\Omega(C_L \sin\phi + C_D cos\,\phi)\delta r \tag{3.35}$$

Figure 3.11 shows the F_{tan} and F_{ax} on a wind turbine.

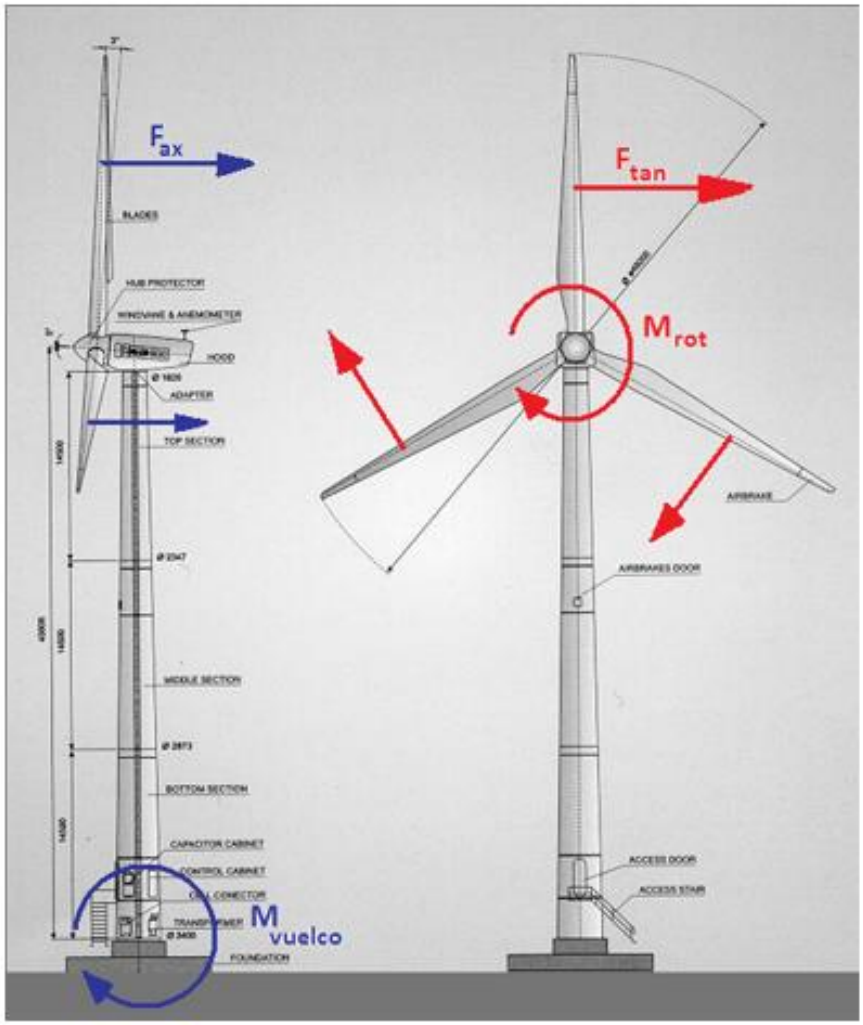

Figure 3.11: Forces on a wind turbine, [7]

3.6.2. BEM Theory

The basic assumption of the BEM theory is that the force of a blade element is solely responsible for the change of axial momentum of the air which passes through the annulus swept by the element. It is, therefore, to be assumed that there is no radial interaction between the flows through contiguous annuli, [9].

Taking into account these specifications and combining the equations developed in the actuator disc and rotor disc theories with the blades element theory, it is obtained

$$\frac{a}{1-a} = \frac{C_L \cos\varphi + C_D sin\varphi}{4sin^2\varphi}\left(\frac{cB}{2\pi r}\right) \tag{3.36}$$

$$\frac{a'}{1+a'} = \frac{C_L \sin\varphi + C_D cos\varphi}{4sin\varphi cos\varphi}\left(\frac{cB}{2\pi r}\right) \tag{3.37}$$

Essentially, these equations above are used to design the wind turbine blades through an iterative process. Blade element momentum theory is utilized to determine the shape of the blade because it allows to find a twist, chord and airfoil configuration for the specifications required about the wind turbine desired.

3.7. Aerodynamic Concept of Wind Turbine

3.7.1. Aerodynamic flow

As airflow moves past the wind turbine, the molecules of the fluid near it are disturbed, introducing the concept of boundary layer and forcing blades to move. This creates a thin layer of fluid near the surface called boundary layer in which the velocity changes from zero at the surface to the free stream value away from the surface, [13].

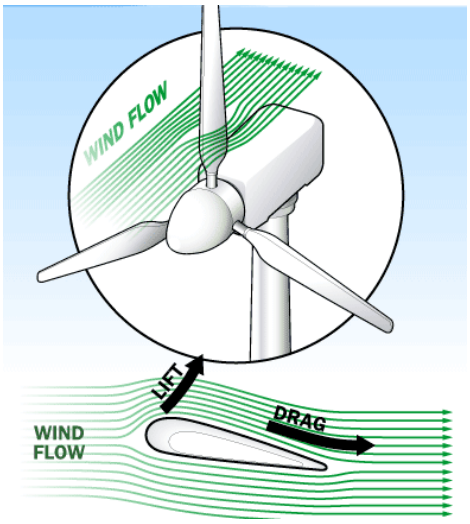

Figure 3.12: Airflow through a wind turbine, [14]

The boundary layer is studied to analyze the variation of velocities in the contact zone between the fluid and a solid. The presence of this layer is mainly due to the existence of the viscosity, inherent property of any fluid. Varying speeds, as the Bernoulli principle, involves a variation in the fluid pressure, which may lead to impact forces such as lift and drag, (see Figure 3.12).

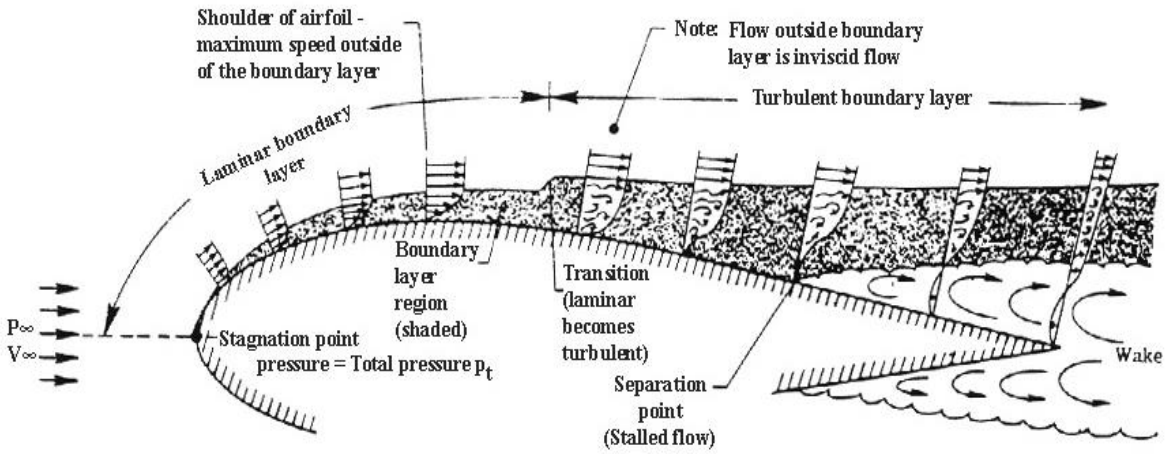

Figure 3.13:.Real fluid about an airfoil, [15]

Figure 3.13 shows the boundary layer of an airfoil. Initially, near the leading edge the airflow is laminar, but it is decelerated along the downstream because of the viscosity. The laminar boundary layer reaches to a transitional point in which it becomes a turbulent boundary layer with random motion. Finally the turbulent flow stops or reverses, causing the boundary layer breaks loose and flow no longer follow the shape of the surface. Thus, flow field is disrupted because of viscosity to extent that a pressure drag arises, [15]. This phenomenon is not desirable because wind turbines using the lift force to extract energy instead of the drag force.

A dimensionless quantity called Reynolds number is widely used to predicting flow patterns in different fluid situation and it also has an important effect on the boundary layer. Laminar flow is related with low Reynolds numbers and it is characterized by smooth and constant fluid, while turbulent flow occurs at high Reynolds numbers and shows chaotic eddies and vortices, [16].

$$Re = \frac{inertial\ force}{viscous\ force} = \frac{U \cdot L}{\nu} = \frac{U \cdot L \cdot \rho}{\mu} \tag{3.38}$$

where U and L are the velocity and length that characterize the scale of the flow, ν is the kinematic viscosity, ρ is the fluid density and μ is fluid viscosity.

In wind turbines, generally are chosen airfoils which generate a turbulent boundary layer in order to delay that the boundary layer breaks loose. The behavior of the airflow around the wind turbine blades is described in the Figure 3.14. The effects of the boundary layer on lift are contained in the lift coefficient and the effects on drag are contained in the drag coefficient, whose formulas are detailed below.

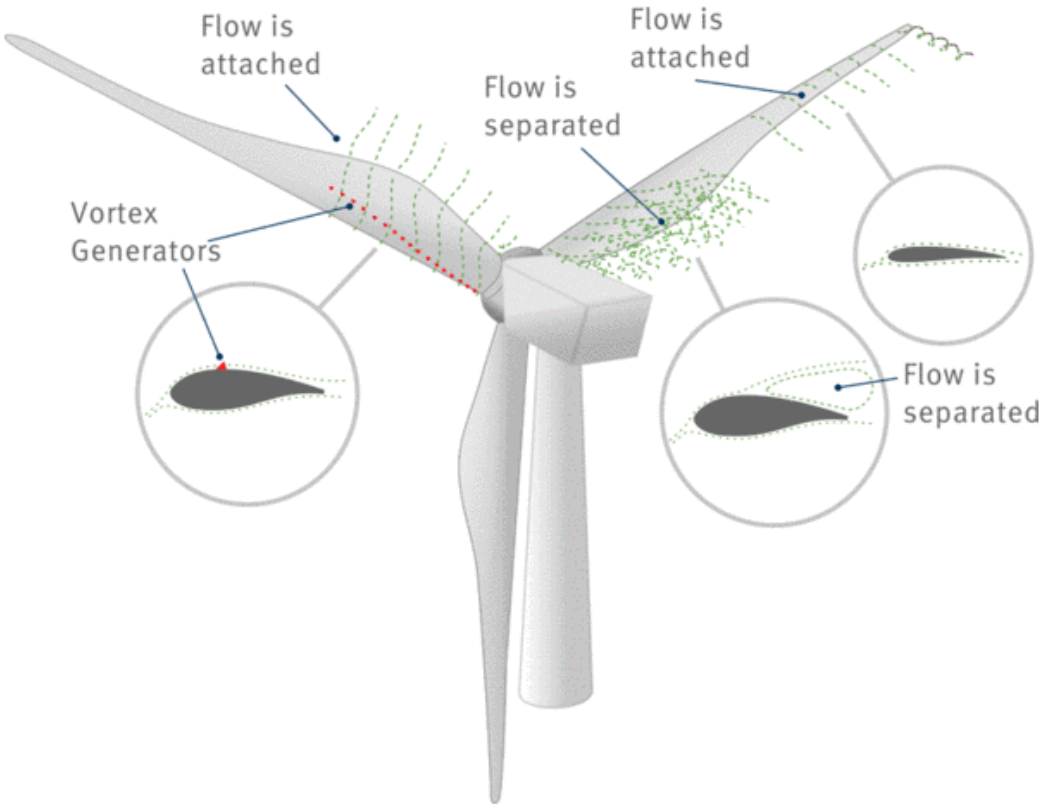

Figure 3.14: Airflow around the wind turbine blades, [17]

3.7.2. Aerodynamic forces

The transmission of mechanical forces between a solid body and a fluid is at every point on the surface of the body and it occurs through the fluid pressure. In the case of a wind turbine, the action of the relative wind which it is composed by the natural wind plus wind caused by rotor motion and rotor-induced flow, generates an aerodynamic force on the rotating blades.

The reacting force F is decomposed into a perpendicular and a parallel direction to the relative wind (W), calling these components lift (L) and drag (D), respectively. The lift is the force used to overcome gravity. Besides, these forces depends on the angle between the chord line of the blade and the relative wind, which is termed the angle of attack.

These forces are given by

$$L = \frac{1}{2} c_L \rho A W^2 \quad [N/m]; \quad C_L = \frac{L/l}{\frac{1}{2}\rho c W^2} = \frac{Lift\ force/unit\ length}{Dynamic\ force/unit\ lenght} \tag{3.39}$$

$$D = \frac{1}{2} c_D \rho A W^2 \quad [N/m]; \quad C_D = \frac{D/l}{\frac{1}{2}\rho c W^2} = \frac{Drag\ force/unit\ length}{Dynamic\ force/unit\ lenght} \tag{3.40}$$

where ρ is the density of air, $c_L$and c_D are the lift and drag coefficients, respectively; and finally, c is the length of the airfoil (denoted also by chord). The forces and velocities over the profile are represented in Figure 3.15, below.

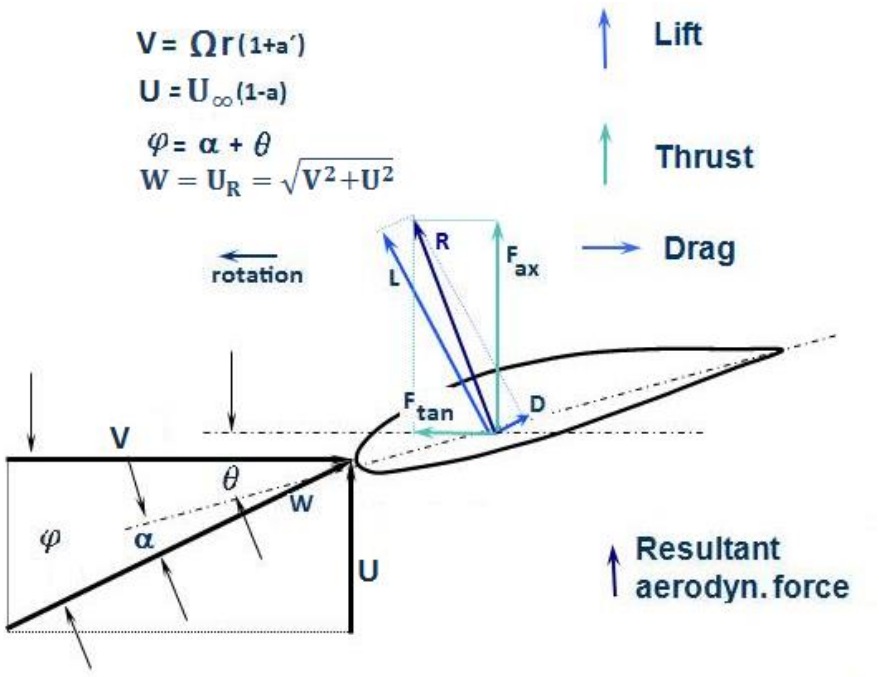

Figure 3.15: Forces and velocities over the profile, [7]

3.8. Problem Specification

Making of analytical models using a series of parameters or variables allows an easier simulation of the element's behavior. One critical task in any wind power studies involves the accurate modelling of the fluid passing around wind turbines blades. The airflow at the turbine hub is different than the airflow at the tip of the blades and further downstream the turbine. However, Computational Fluid Dynamics (CFD) analysis and powerful computers with high memory capacity are now available, thus make it possible to simulate flow effects on wind turbines.

But even using CFD codes, the aerodynamics of HAWT are still not straightforward. Hence, the motivation of this project consist of studying the behavior of the wind turbine blades comparing the results obtained according to the theory and using ANSYS, in order to demonstrate how these models can be used to study wind turbine operation issues.

Furthermore, they also can be utilized to perform real studies in the industry during the preliminary stage of design of HAWT blades, making the studies more powerful and less tedious than using classical aerodynamic theories. The results calculated using classical aerodynamic theories are compared with the numerical results from the software in order to evaluate them and calculate the errors committed.

From a modelling standpoint, wind turbines may be represented as an interaction between aerodynamic, mechanical, and electrical components; as illustrated in Figure 3.16, which shows the four building blocks required. The electrical and the control blocks are not going to develop in this project, just only being mentioned according to a global vision of the problem.

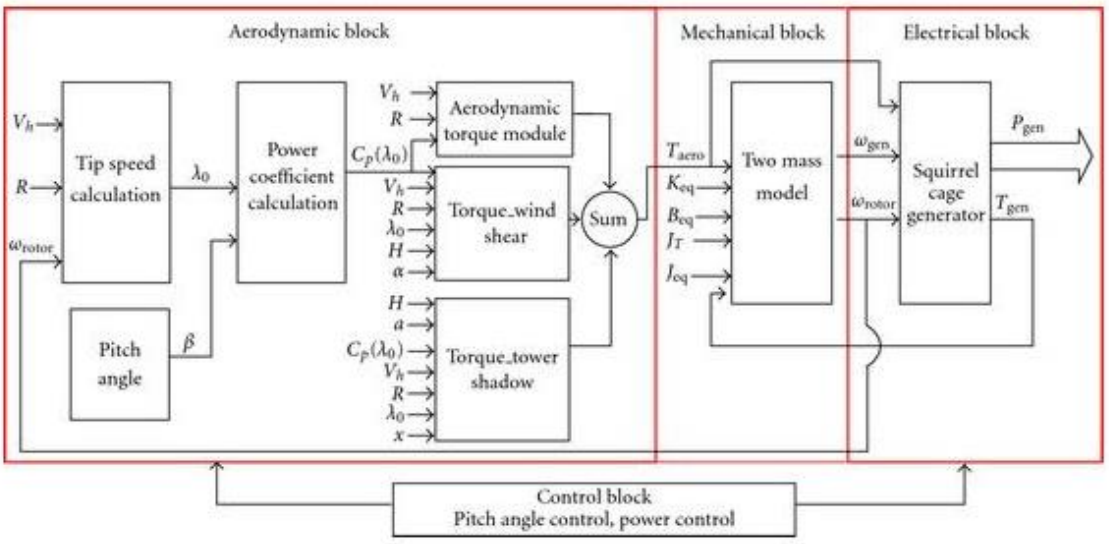

Figure 3.16: Block diagram of a wind turbine, [18]

Before starting to define the mathematical characteristics of the project, it is essential to describe the procedure followed. Simulations of a suitable aerodynamic model have been developed using *Fluent* and *Mechanical* included in the software ANSYS. The analyses are divided in two parts, based on the tutorial about the deformation of a wind turbine blade, contained in the web of the Cornell University. Part 1 of the tutorial uses *ANSYS Fluent* to develop the aerodynamics loading on the blade. In part 2, *ANSYS Mechanical* is used to determine stresses and deformations on the blade.

This project aims to undertake aerodynamic analysis of a downwind horizontal axis wind turbine (HAWT), which has a rotor made up of three blades. Each one is 42.3 meters long and starts with a cylindrical shape at the root and then transitions to the airfoils S818, S825 and S826 for the root, body and tip, respectively, [19].

Nowadays, the majority of the airfoils used in HAWTs are originally developed for aircraft. Such airfoils family called NREL is chosen because it is designed specifically for horizontal axis wind turbines as they reduce annual energy losses caused by the roughness, with respect to the airfoils previously used in wind turbines. The profiles known as NACA (National Advisory Committee for Aeronautics) series have been discarded as a result of the fast deterioration of their performance characteristics when their thickness increased, [20]. Figure 3.17 shows the NREL families.

Diameter	Type	Thickness Category	Airfoil		
			Primary	Tip	Root
2–10 m	Variable speed Variable pitch	Thick		S822	S823
10–20 m	Variable speed Variable pitch	Thin	S801	S802 S803	S804
	Stall regulated	Thin	S805 S805A	S806 S806A	S807 S808
	Stall regulated	Thick	S819	S820	S821
20–30 m	Stall regulated	Thick	S809	S810	S811
	Stall regulated	Thick	S812	S813	S814 S815
20–40 m	Variable speed Variable pitch	—	S825	S826	
30–50 m	Stall regulated	Thick	S816	S817	S818

Figure 3.17: NREL families of profiles, [20]

The blade also has pitch to vary as a function of radius, giving it a twist and the pitch angle at the blade tip is 4 degrees. It was created to be similar in size to a GE 1.5XLE turbine whose specification sheet is included in the annexes, it is made of orthotropic composite material and it has a varying thickness. The spar inside provides rigidity to the blade, [19].

According to behavior of the wind, it is considered turbulent flow towards the negative z-direction whose value is assumed $12\,m/s$ as it is shown in the Figure 3.18. Besides, it makes the blade rotate at an angular velocity of -2.22 rad/s about the z-axis and the tip speed ratio is 8, all of them reasonable values for a turbine of this size.

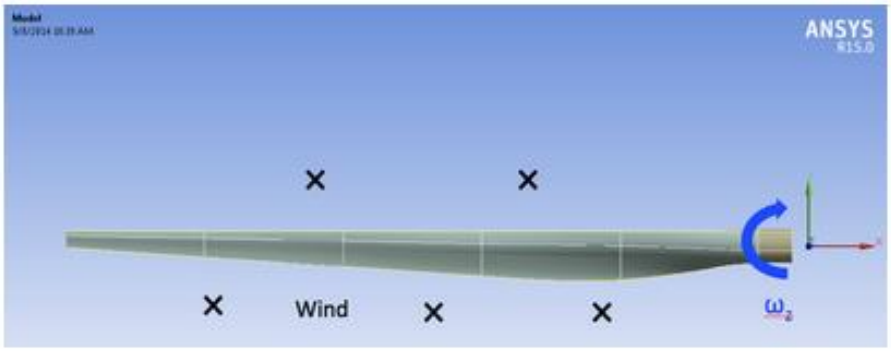

Figure 3.18: Blade in ANSYS, [1]

Chapter 4

Aerodynamic Model of Wind Turbine

4.1. Introduction

Despite being a relatively new technology, there are a considerable amount of resources and important engineering information which are being used for research on harnessing the wind energy efficiently. Out of all the factors considered in these studies, an accurate wind turbine blade design is essential in order to improve the efficiency.

According to [9], a successful blade design must satisfy a wide range of objectives, which are summarized as follows:

1. Maximize annual energy yield for the specified wind speed distribution.
2. Limit maximum power output (in case of stall regulated machines).
3. Resist extreme and fatigue loads.
4. Restrict tip deflections to avoid blade/tower collisions (in the case of upwind machines).
5. Avoid resonances.
6. Minimize weight and cost.

The design process can be divided into two stages: the aerodynamic design, in which objectives 1 and 2 are satisfied, and the structural design (the latter is detailed in chapter 5). The aerodynamic design encompasses the concept of the blade geometry, defined by the airfoil family and the chord, twist and thickness distributions. Besides, it is also related with the behavior between the airflow and blades.

This project uses ANSYS software in order to carry out the two stages. First of all, the blade geometry is performed in CAD following the data detailed in [19]. Then, aerodynamic design is developed and finally, the structural model. See Figure 4.1 which describes the process followed.

This chapter intends to understand the steady aerodynamics associated with wind turbines by performing CFD simulations of the flow past a wind turbine. BEM is a quite commonly method used to study the aerodynamic part. However, there are others as CFD models, which are more sophisticated and computationally much more expensive. Both are being developing and then, a comparison between them are included in the conclusions part of the project.

Even using CFD codes, the flow over wind turbines is still a challenging numerical problem because it must take into account factors as variation of the flow parameters in length scales, turbulent flow over the blade sections, complicated blade geometry with changes in angle of attack and so on.

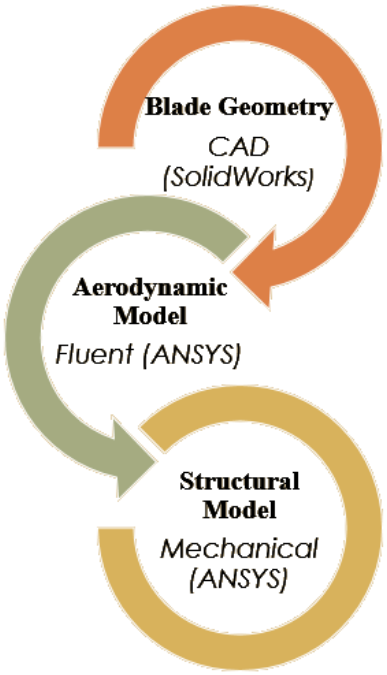

Figure 4.1: Process followed in the project

Hence, it is necessary to understand carefully the blades environment which is defined by wind speeds and boundary conditions of the domain, as well as by their external morphology related with the dimensions. It is based on the first part of the tutorial mentioned above in the previous chapter and the overwhelming majority of the initial data are detailed in section 3.1 called Problem Specification. Figure 4.2 below shows the initial screen of ANSYS Fluent and all the sections which are described in the followings points of the chapter.

All this information is introduced in ANSYS Fluent following some steps fixed by the software (see Figure 4.2). As explained before, ANSYS software is chosen because it allows carry out Computational Fluid Dynamics (CFD) simulations in order to investigate in detail inside the fluid domain around the blade virtually, not physically. Besides, it develops mesh simulations and improves outcomes testing changes in parameters that would be impossible to do in a short period of time otherwise.

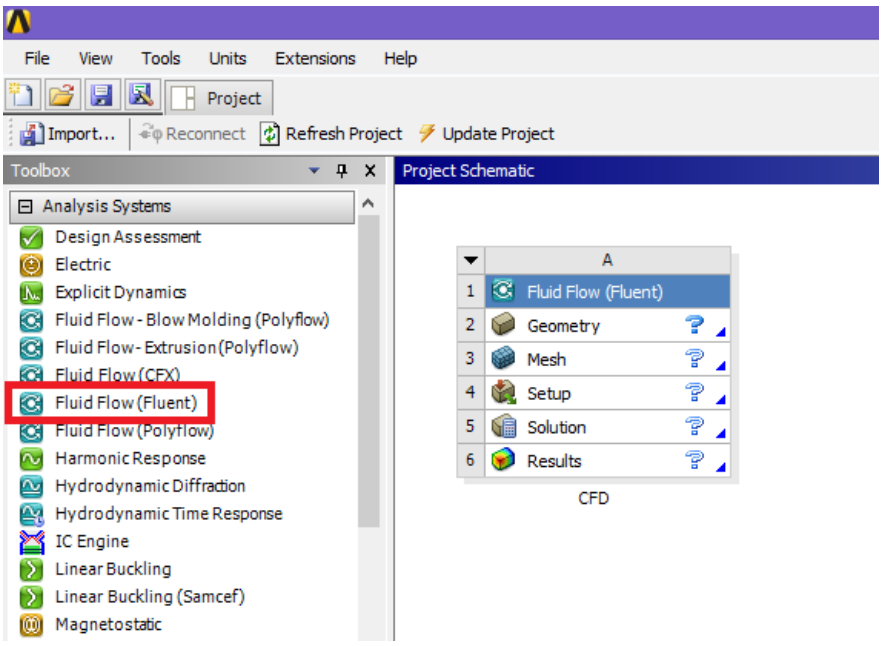

Figure 4.2: Initial screen from ANSYS Fluent

4.2. Geometry

The first step in ANSYS Fluent is denoted as Geometry and its aim is drawing the fluid domain. It is modelled only the 1/3 of the full domain using periodicity assumptions, described in the Figure 4.3 below, [19]. Following this assumptions, only one of the blades is represented.

Inside Geometry part, the blade geometry is imported. It is important to note that using CFD analysis, the body must be locked in a virtual wind tunnel, where the boundary conditions are applied. The boundary conditions on the fluid domain are showed in Figure 4.4 and described as follow:

- Inlet: Velocity of $12\ m/s$ with turbulent intensity of 5% and turbulent viscosity ratio of 10.
- Outlet: Pressure of 1 atm.
- Blade: No-slip.
- Side Boundaries: Periodic.

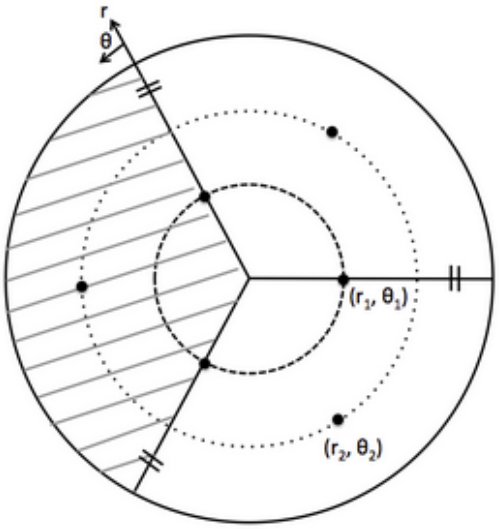

$$\vec{v}(r_1,\theta) = \vec{v}(r_1,\theta_1 - 120°n) \quad \text{For n = 1, 2, 3...}$$
$$= \vec{v}(r_1,240° - 120°(1)) = \vec{v}(r_1,120°)$$
$$= \vec{v}(r_1,240° - 120°(2)) = \vec{v}(r_1,0°)$$

$$\vec{v}(r_2,\theta) = \vec{v}(r_2,\theta_2 - 120°n) \quad \text{For n = 1, 2, 3...}$$
$$= \vec{v}(r_2,180° - 120°(1)) = \vec{v}(r_2,60°)$$

Figure 4.3: Periodicity assumptions, [19]

Once drawn the fluid volume using sketches, it is necessary to indicate its material as a fluid instead of solid in the software and then, subtract the blade from the fluid body.

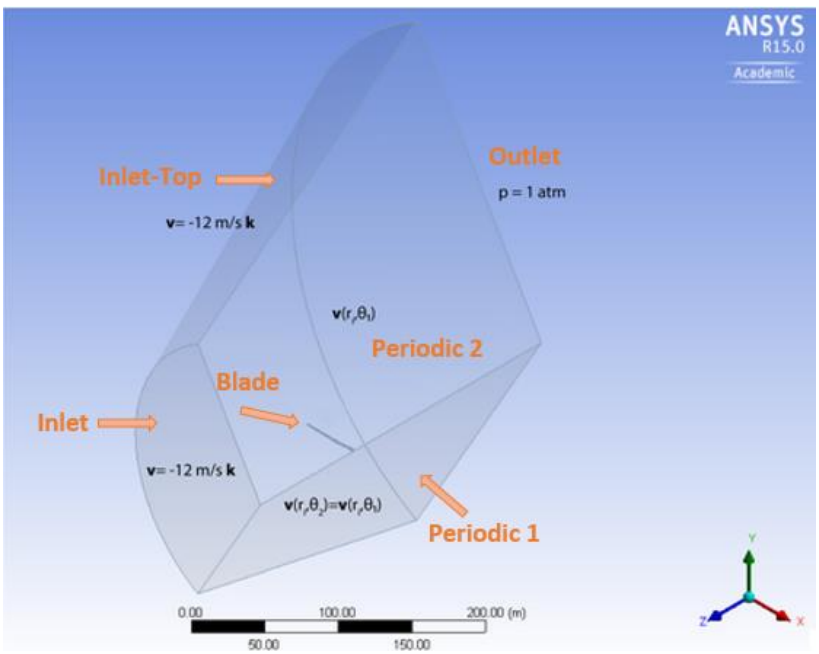

Figure 4.4: Fluid domain modelling in ANSYS Fluent

4.3. Mesh

The second step is creating the Mesh. Meshing is a discrete representation of the geometry and it involves grid generation and converting the grid into a format which can be understood by the CFD solver. Essentially, it partitions space into elements or cells over which the equations can be approximated. Mesh is represented in Figure 4.5, below.

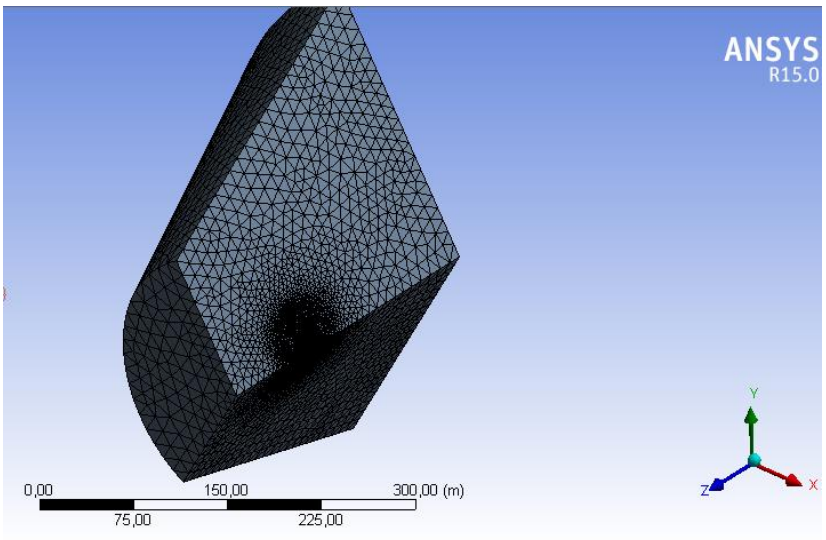

Figure 4.5: Mesh part in ANSYS Fluent

Fluent converts the differential equations based on the governing equations (continuity and Navier-Stokes) into a set of algebraic equations. Actually, the surface wrapping algorithm quickly creates an airtight envelope based on the selected bodies. Inverting these algebraic equations gives the value of (u, v, w, p, k, and ω) at the cell centers, [19]. Hence, the total number of cells in the mesh are around 400,000 cells, (see Figure 4.6).

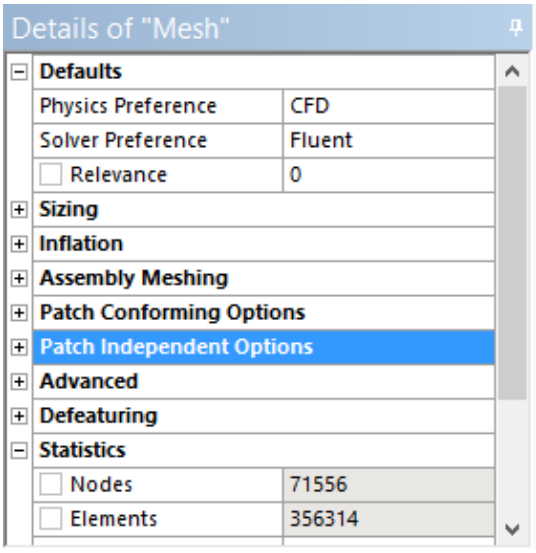

Figure 4.6: Details of the Mesh in ANSYS Fluent

This project uses structured grids based on a collection of regular repeating elements, represented by tetrahedral elements in 3D. A tetrahedron has 4 vertices, 6 edges, and it is bounded by 4 triangular faces (see Figures 4.5 and 4.7), so the fluid domain is generated automatically as tetrahedral shaped.

Creating an accurate mesh is the most critical step in the simulation because the mesh quality can be conclusively. The density of the mesh is required to be sufficiently high in order to capture all the flow features but at the same time, it must ensure that no unnecessary details of the flow are calculated because the CPU can be burdened.

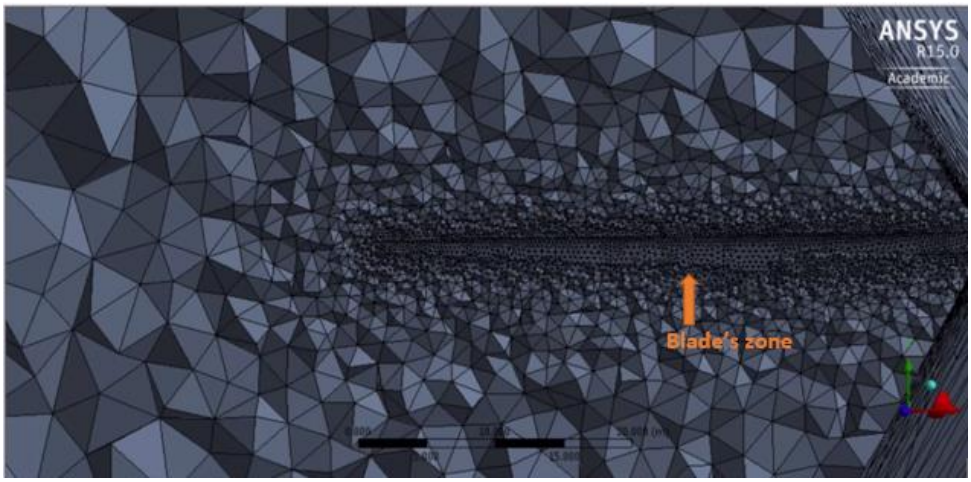

Figure 4.7: Tetrahedral shaped cells in ANSYS Fluent

Getting good quality (less skewed elements) required a fair amount of experience, time and effort. Hence, in order to improve the overall accuracy of the CFD solution, these grids can be made finer by stretching in a particular direction, getting lower skewness using an advanced size function to proximity and curvature. The relevance center is also changed to medium, (see Figure 4.8).

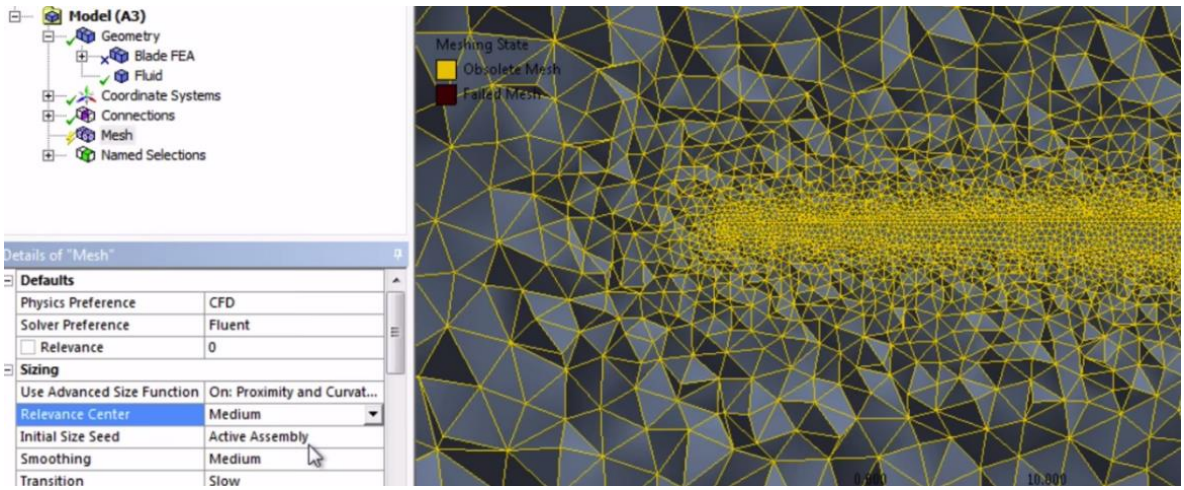

Figure 4.8: Results of changing Advanced Size Function as a Proximity and Curvature and Relevance Center to medium in ANSYS Fluent

It is extremely important to judge the quality of the mesh, because using the rough grid mesh (with less cell) can lead to incorrect simulation results, as it is written before. Studies as skewness and orthogonal quality are chosen. Generally, it is advised to keep the minimum orthogonally greater than 0.15 and maximum skewness lower than 0.95, (see Tables 4.1 and 4.2), [19].

Table 4.1: Skewness range values

Skewness:

Outstanding	Very Good	Good	Sufficient	Bad	Inappropiate
0-0.25	0.25-0.50	0.50-0.80	0.80-0.95	0.95-0.98	0.98-1.00

Table 4.2: Orthogonal quality range values

Orthogonal Quality:

Outstanding	Very Good	Good	Sufficient	Bad	Inappropiate
0.95-1.00	0.70-0.95	0.20-0.70	0.15-0.20	0.001-0.15	0-0.001

Figure 4.9 illustrates the skewness study obtained by using the data of the model. Evaluating the skewness analyses data have been done taking into account the range of values presented in Table 4.1. According with this explanation, there is an evidence that the results represented in the graphic below are adjusted with the outstanding and very good range values of the skewness analyses.

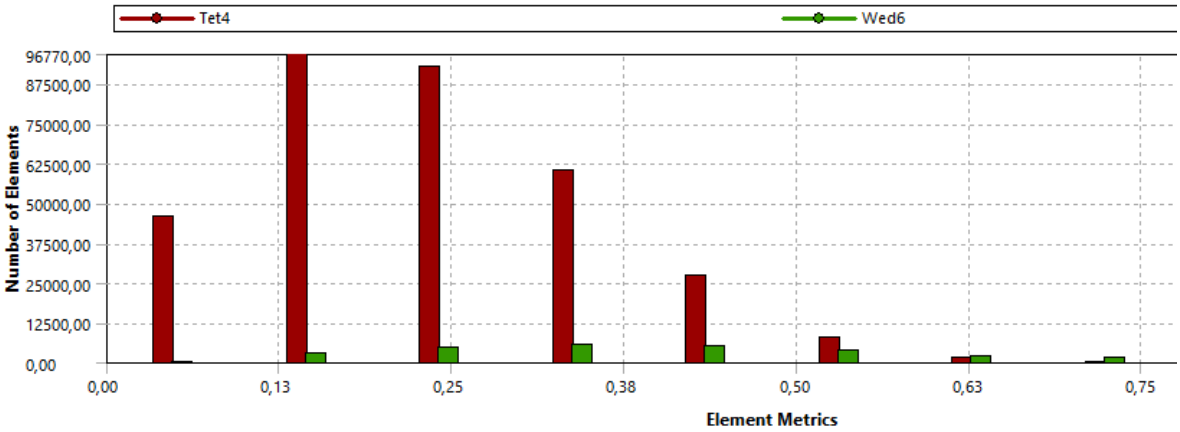

Figure 4.9: Skewness in ANSYS Fluent

Figure 4.10 describes the orthogonal quality study and it shows that the data complies the requirements of the outstanding and very good range values of this analyses, which are detailed in Table 4.2.

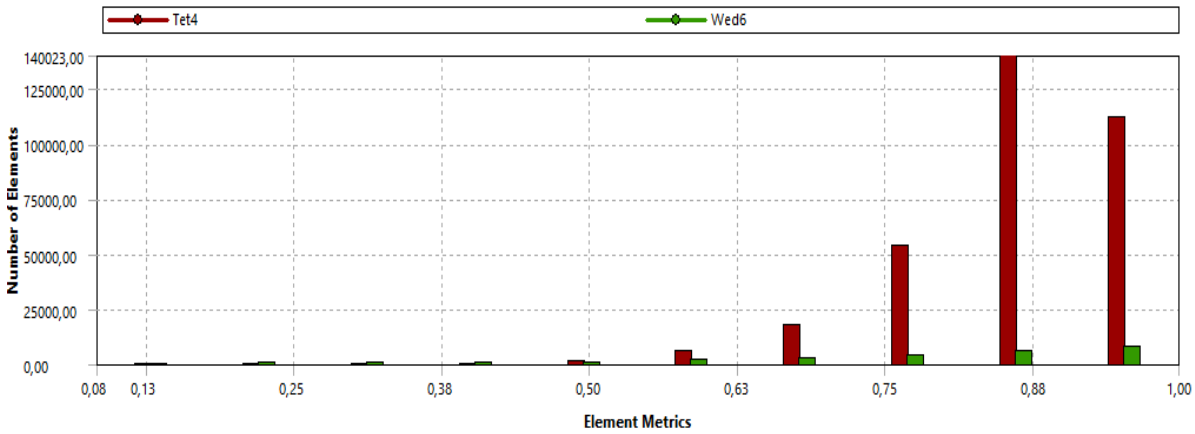

Figure 4.10: Orthogonal Quality in ANSYS Fluent

4.4. Physics Setup

This section is concerned with the physics governing equations. First of all, a few settings must be specified such as the precision and the procession options.

Double precision is selected in order to get a more accurate solution. Between the two different processing options, the serial option uses only one core to solve the solution and it is likely the best choice for small models. However, aerodynamic model of wind turbine blades is considered a large model, because of the huge number of cells which conform the mesh. Hence, the parallel option is chosen. This one allows to use multiple cores in order to solve the numerical problems in a faster way and because of that, it is typically the best option for large models. All these settings are shown in Figure 4.11.

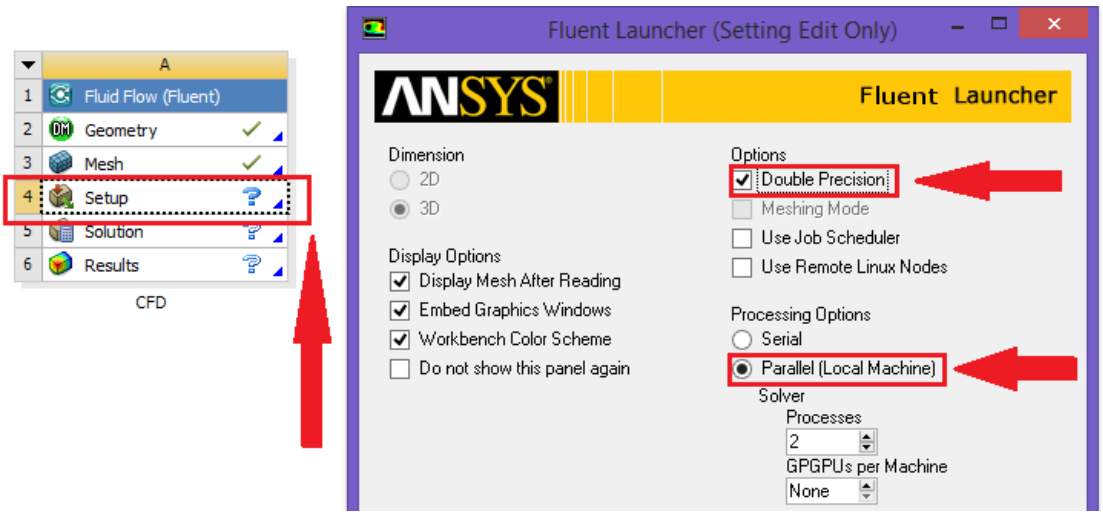

Figure 4.11: Setup settings in ANSYS Fluent

Afterwards, the conditions which affect the mathematical model of this specific problem are established. The CFD solver uses a steady time, pressure-based type and absolute velocity formulation, (see Figure 4.12). The concept of steady state is related with dynamic equilibrium. This means that the properties of the airflow, such as ρ and the pressure, are unchanging in time. Pressure-based type and absolute velocity formulation are chosen because the data of boundary conditions of the model (see Section 4.2) are based on these magnitudes.

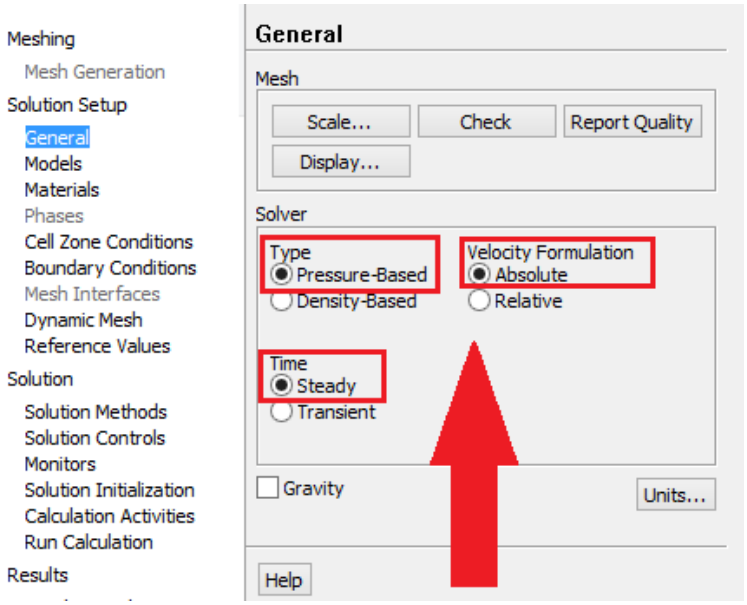

Figure 4.12: Solution setup general settings in ANSYS Fluent

The airflow behavior is considered as a fluid which follows the features of the viscous model called SST k-ω turbulence model, (see Figure 4.13). Turbulence is the most complicated kind of fluid motion because it involves a three-dimensional, time-dependent and nonlinear phenomenon and it is modelled by using the Navier-Strokes equations.

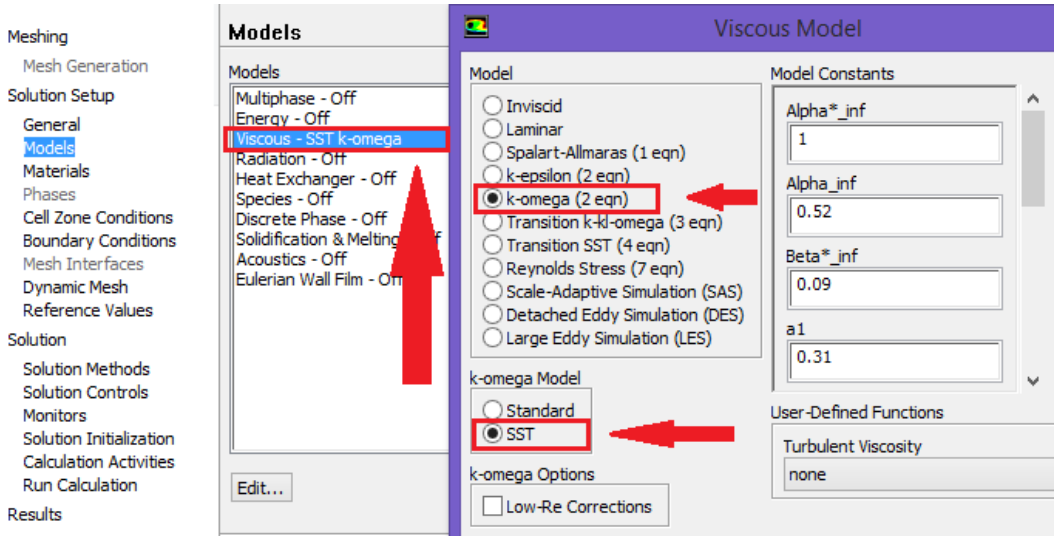

Figure 4.13: Viscous model settings in ANSYS Fluent

The k– ω Shear Stress Transport (SST k– ω) formulation combines two equations based on k– ω model in order to represent two turbulence properties of the flow. The first one is the turbulence kinetic energy (k) and the second is the specific dissipation rate (ω). Navier-Strokes formulation is described as

$$\frac{\partial \vec{V}}{\partial t} + (\vec{V}\vec{\nabla})\vec{V} = \vec{f} - \frac{1}{\rho}\nabla p + \vartheta \Delta \vec{V} \tag{4.2}$$

The two equations based on k– ω model are

$$\frac{\partial}{\partial t}(\rho k) + \frac{\partial}{\partial x_i}(\rho k u_i) = \frac{\partial}{\partial x_j}\left(\Gamma_k \frac{\partial k}{\partial x_j}\right) + G_k - Y_k + S_k \tag{4.2}$$

$$\frac{\partial}{\partial t}(\rho w) + \frac{\partial}{\partial x_i}(\rho w u_i) = \frac{\partial}{\partial x_j}\left(\Gamma_w \frac{\partial w}{\partial x_j}\right) + G_w - Y_w + D_w + S_w \tag{4.3}$$

where $\nu = \frac{\mu}{\rho}$ is coefficient of kinematic viscosity. In equation (4.1) $\vec{f}$ is the distributed volumen force.
G_k represents the generation of turbulence kinetic energy due to mean velocity gradients;
G_w represents the generation of ω;
Γ_k , Γ_w represents the effective diffusivity of k and ω;
Y_k , Y_w represents the dissipation of k and ω;
D_w represents the cross-diffusion term;
S_k , S_w are user-defined source terms.

The turbulent viscosity follows

$$\mu_t = \frac{\rho k}{w} \frac{1}{max\left[\frac{1}{\alpha^*}, \frac{SF_2}{a_1 w}\right]} \tag{4.4}$$

Specific rate of dissipation (SDP) is *SDP(1/s) = 0.6388766*

$$\Gamma_k = \mu + \frac{\mu_t}{\sigma_k} \qquad \Gamma_\omega = \mu + \frac{\mu_t}{\sigma_w}$$

and

$$G_k = \min(G_k, 10\rho\beta^* k\omega) \qquad G_w = \frac{\alpha}{\nu_t} G_k$$

$$Y_k = \rho\beta^* k\omega \quad ; \quad Y_k = \rho\beta\omega^2$$

, where β and β^* are constants

The advantages of *k-ω SST* turbulence model over the Standard model *k-ω* are*:*

- the possibility of inclusion the diffusion terms in the equations describing specific dissipation of the TKE (turbulent kinetic energy), equation (4.3) from the upper system;
- the possibility of determination the turbulent fluctuations in the turbulent flow by calculating the turbulent viscosity;

- the possibility of linearization of the equation based on the using of the constant parameters using for simplified the numerical solution;
- the possibility of using in the case of compressible flow;

The *k-ω SST* turbulence model is suitable of using into the simulation of multiphasic turbulent flow.

The main disadvantage of this turbulent model is the complex mathematics that is using to describe the flow field, based on the determination of the values of the basic constants, describing the physical properties of the fluid, [21].

Finally, materials, cells conditions, boundary conditions of the fluid domain and mesh interfaces are selected, as it is shows in Figure 4.14, below.

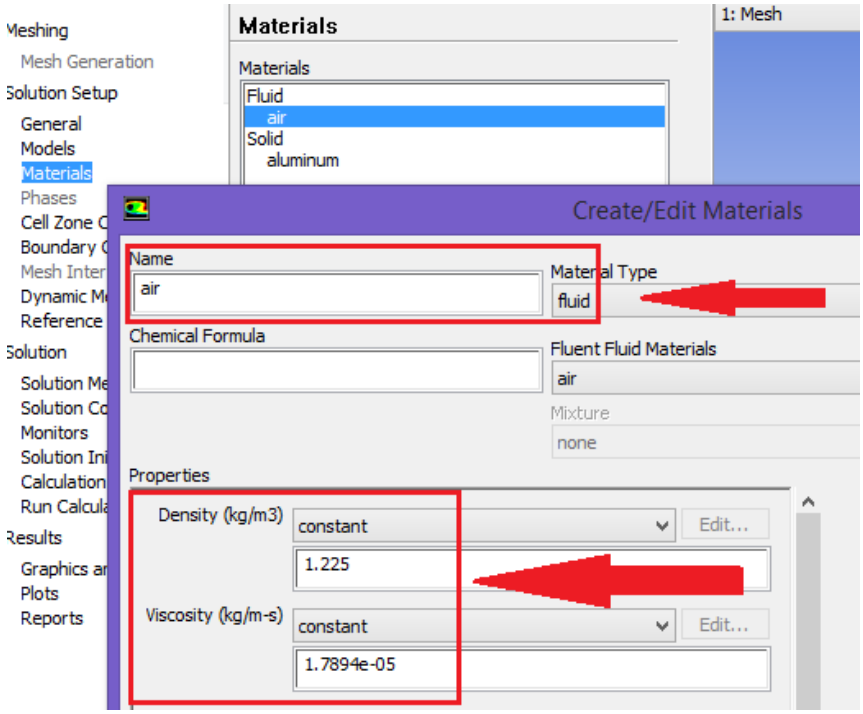

Figure 4.14: Materials selected in ANSYS Fluent

4.5. Solution and Results

A thorough experimental investigation of a wind turbine's aerodynamic behavior should include experimental data. However, when the experimental work is limited because data of the aerodynamic loading distributions along the blades or the wake geometry are unavailable, BEM analysis and the classical theory of aerodynamics can be done to validate the results obtained by using ANSYS.

This chapter describes the calculation of the numerical solution by using the software and also, sets out the last point of the aim, the verification of the numerical results for wind turbine blade tip velocity and wind turbine blade's radial force. It is been performed by comparison of the results obtained by ANSYS with the analytical data calculated by using 1D momentum theory.

From this point, the software is going to calculate the numerical solution though a series of iterations. The solution must be converged in order to ensure that it approaches an accurate result. The number of iterations is chosen by the user and in this case, 1500 iterations could give a good approximation of the real solution, (see Figure 4.15). Note that the time required to perform the solution is directly proportional to the number of iterations. Figure 4.16 describes the time required and the number of iterations left during the run calculation.

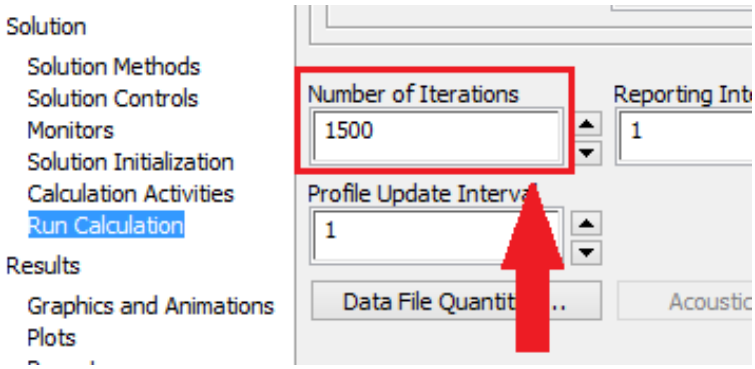

Figure 4.15: Run calculation setting in ANSYS Fluent

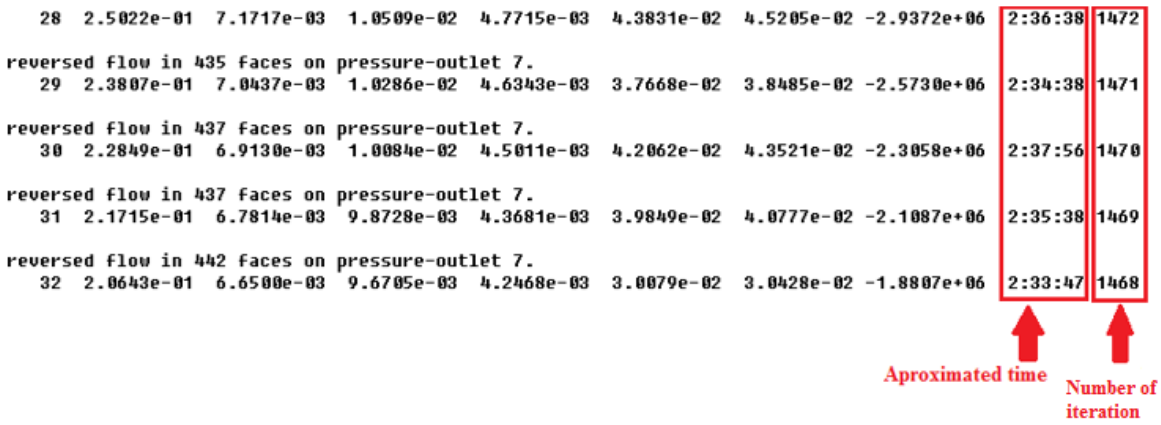

Figure 4.16: Run calculation setting in ANSYS Fluent

Once the 1500 iterations have been completed, it is necessary to determinate whether the solution has converged. One way to doing it is checking the mass flow which implies that the mass conservation equation is complied. The balance of mass flow rate of the airflow is zero between the flow into zone "inlet" and "inlet top' and the zone "outlet".

Figure 4.17 shows that the mass flow net rate is almost zero, so the mass conservation is fulfilled. Converge can also be illustrated by using Figure 4.18, which describes the behavior of the pressure during the iterations. It clearly shows that the pressure approaches a limit value between about negative 7,000 and negative 8,000 Pa. These two studies are enough to proving the veracity of the results.

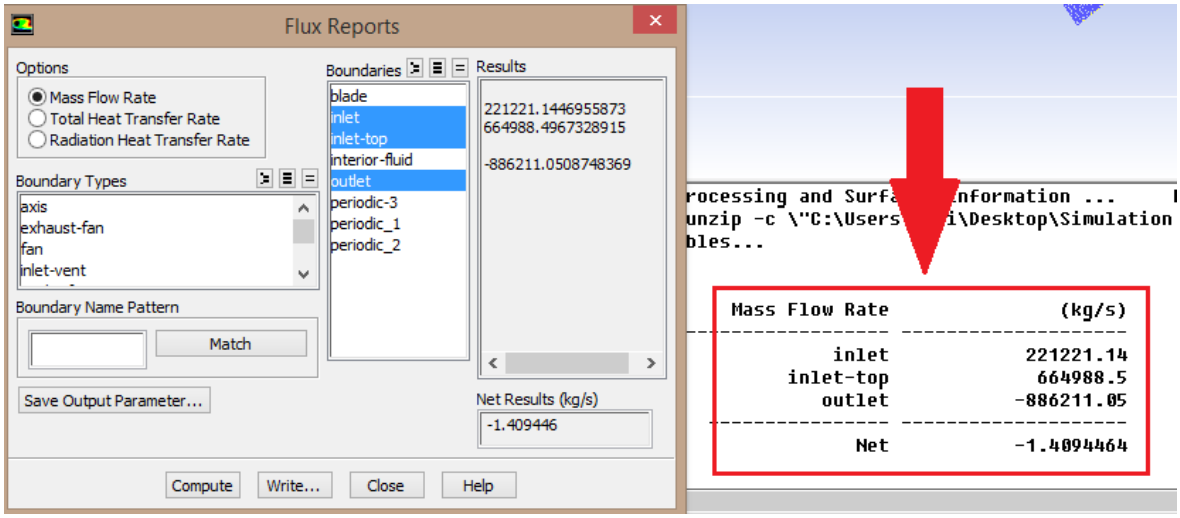

Figure 4.17: Mass flow rate in ANSYS Fluent

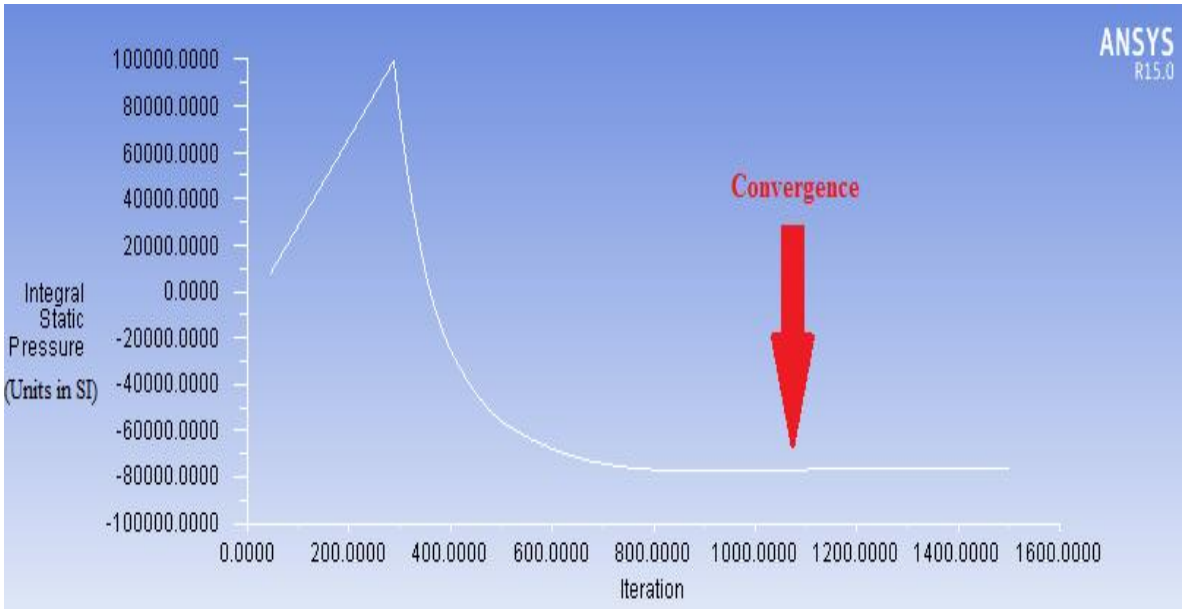

Figure 4.18: Static pressure in ANSYS Fluent

4.5.1. Wind Velocity at the Tip

First, a hand-calculation is done based on the classical aerodynamic theory in order to find the theoretical wind velocity at the tip, [19].
The velocity on the blade follows the formula below

$$u = r\ x\ \omega \tag{4.5}$$

The value of the angular velocity is $-2.22\ rad/s$ and the blade length is $44.2\ m$, taking into account that 1 meter is the distance from the root to the hub. Plugging in these data in the equation (4.1)

$$u = (-44.2\ m)\hat{\imath}\ \ x\ (-2.22\ rad/s)\hat{k} \tag{4.6}$$

$$u = 98.10\ m/s\ \ \hat{\jmath} \tag{4.7}$$

This data is compared with the value of the velocity obtained by ANSYS. Figures 4.19 and 4.20 illustrate that the local wind turbine blade velocity increases with radius because of the rotation of the blades. The velocity of the tip, which is the highest velocity, it is around $98.05\ m/s\ \ \hat{\jmath}$, the same value as equation (4.7).

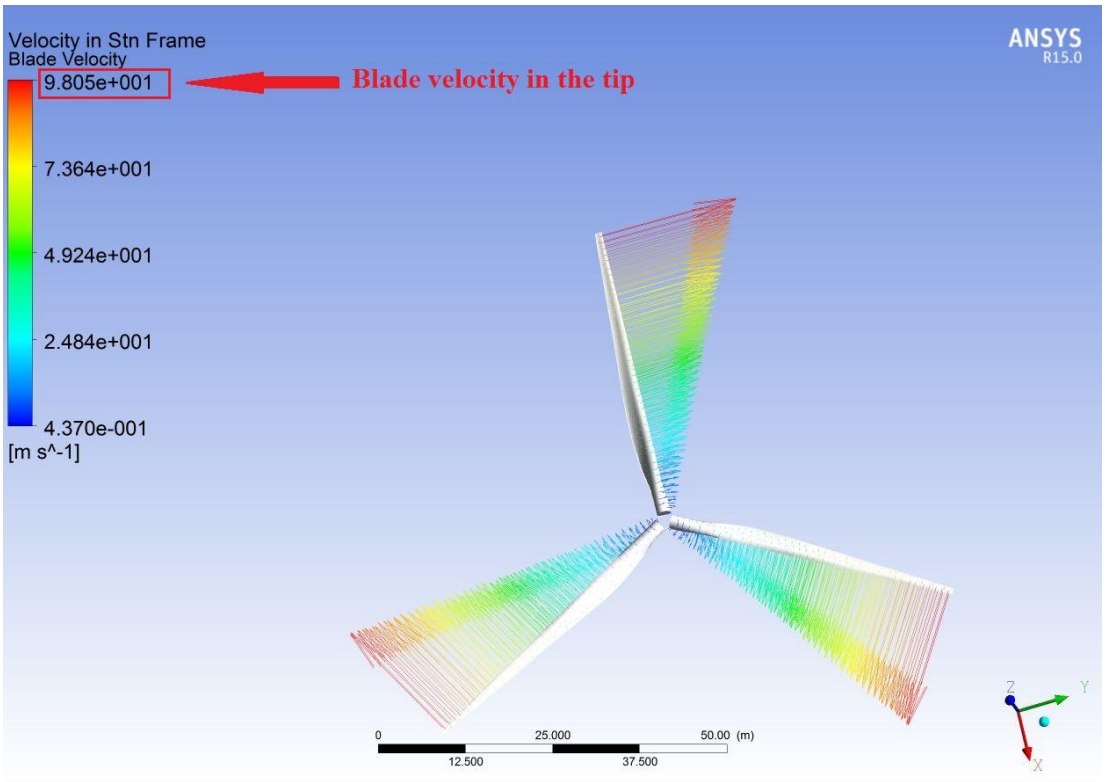

Figure 4.19: Wind turbine blades velocity in ANSYS Fluent

Table 4.3: Wind velocity at the tip

Wind velocity at the tip:

Hand-calculation (m/s)	CFD analysis (m/s)	error (%)
98,10	98,05	0.05

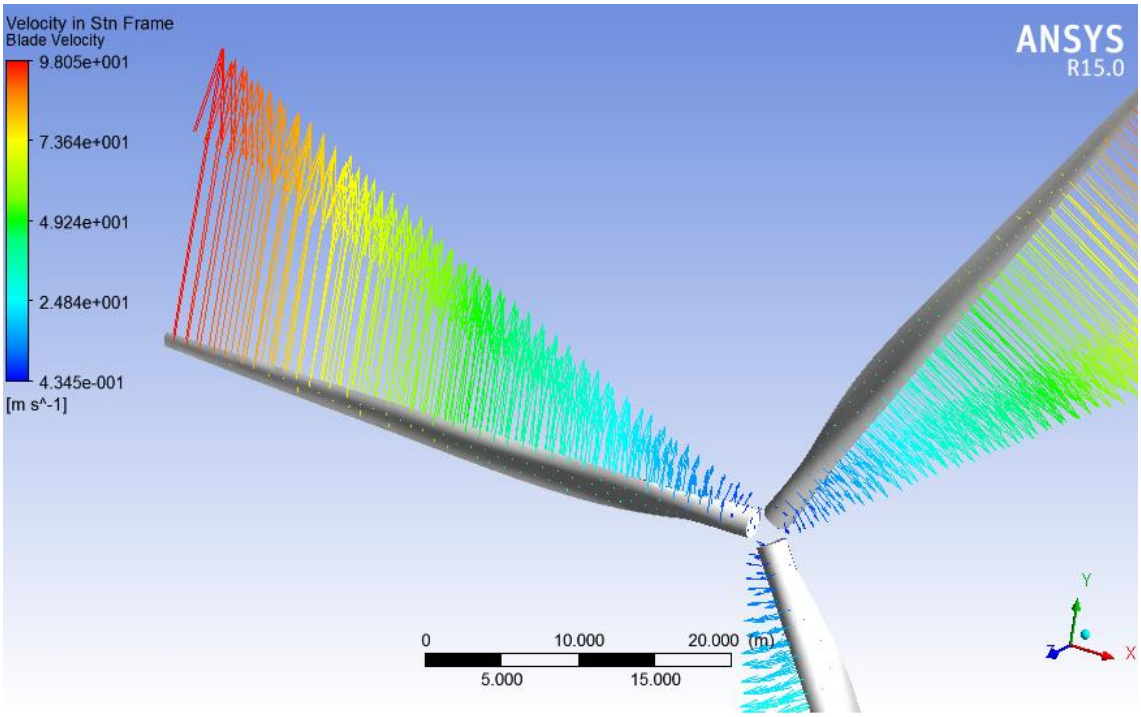

Figure 4.20: Wind turbine blades velocity in detail in ANSYS Fluent

4.5.2. Wind Velocity Streamline

Wind velocity streamline shows the velocity of the fluid domain around the three wind turbine blades, (see Figures 4.21, 4.22 and 4.23).

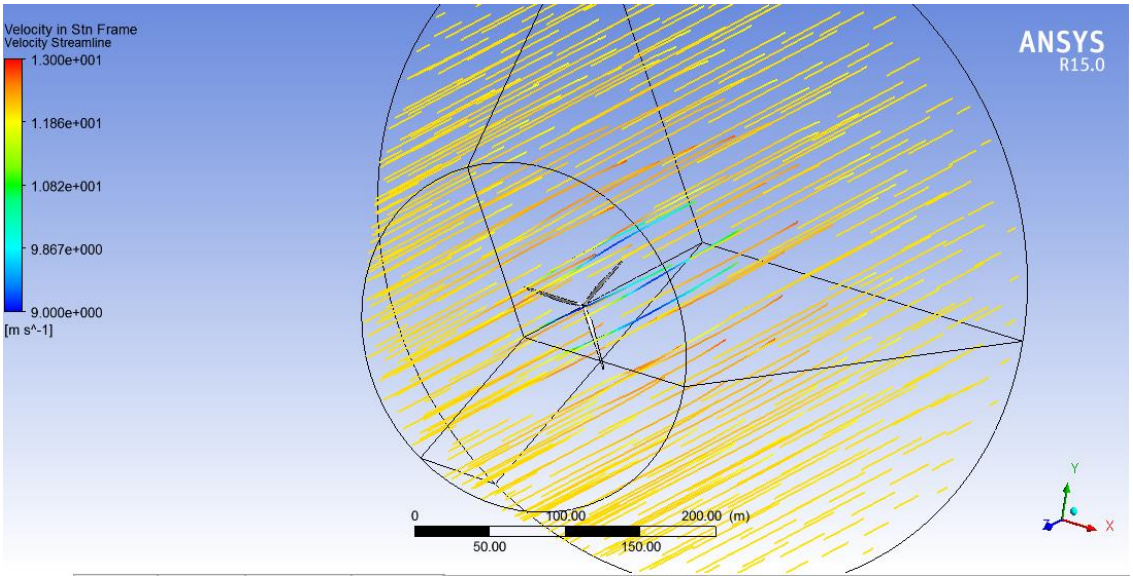

Figure 4.21: Velocity Streamline in ANSYS Fluent

Note that the legend bar in the following pictures presents a color graduation from blue, which is the lowest velocity, until red. Inlet section has yellow color, so it is 12 m/s , as it was written in Section 4.2. The color blue in the streamlines means that when the airflow passes the blades, it suffers a slowing down and the velocity decreases. Clearly, an acceleration of the flow around the wake is represented by red color. All these features match the mass conservation and momentum theory.

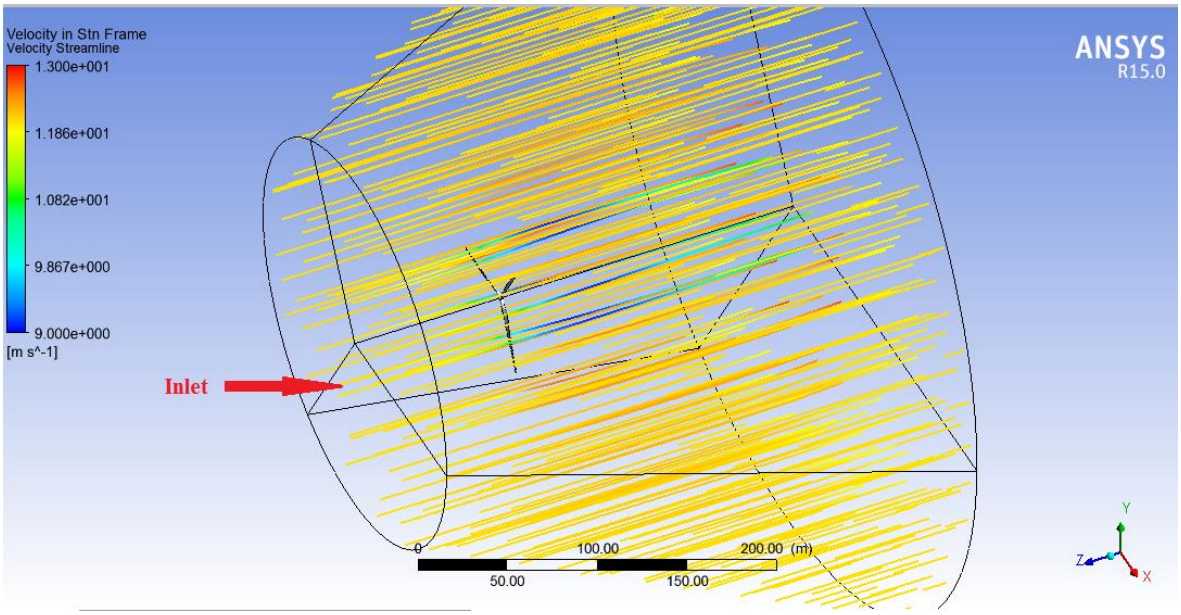

Figure 4.22: Velocity Streamline in ANSYS Fluent

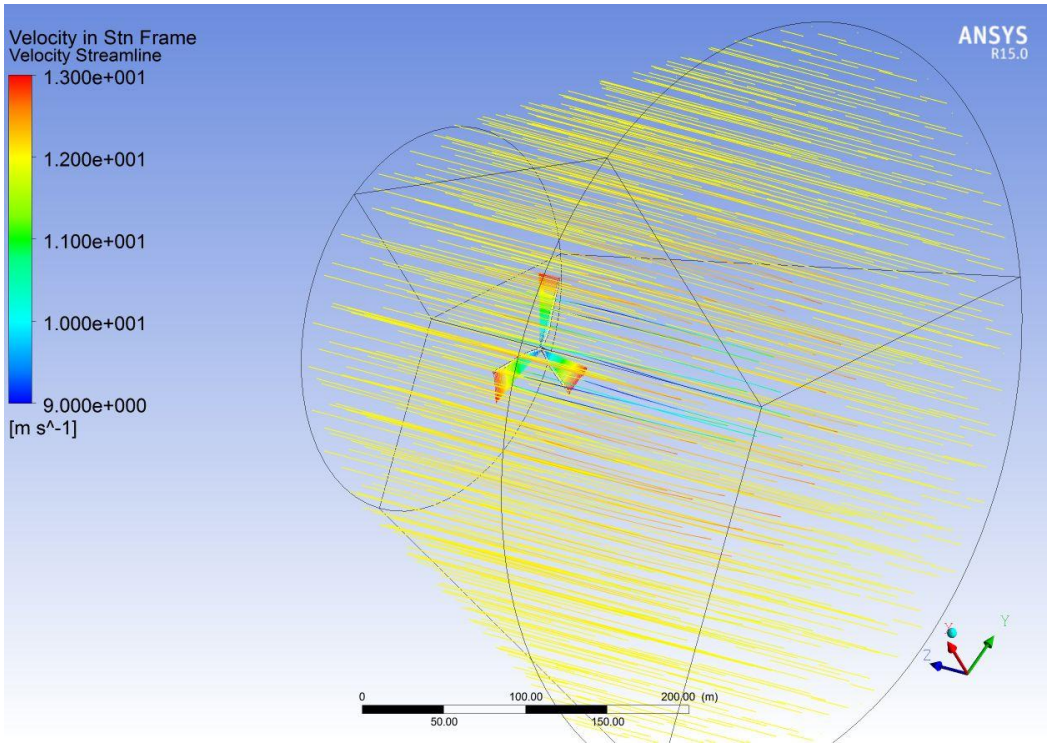

Figure 4.23: Velocity Streamline in ANSYS Fluent

Figure 4.24 describes the airflow velocity before the fluid reaches the blades and after that. This picture is essential in order to sum up the concepts schematically and it uses the same colors specified in the legend before. Yellow arrows show that the airflow arrives to the blades with $12\ m/s$ and afterwards, the fluid suffers a slowdown because of the friction with the surface of the blades. Just the airflow passing the blade which is represented by red arrows increases the velocity, even exceeding the $12\ m/s$. At the tip of the blade, it is observed vortex generation, which causes the additional velocities called induced velocities. For this reason, airflow velocity at this point of the blade is the sum of the velocity at the input plus the velocity induced by the vortex.

It is also related with the pressure. According to Bernoulli equation, the airflow velocity and the pressure are directly related

$$P + \frac{1}{2}\rho u^2 + \rho g h = constant \tag{4.8}$$

Assuming that the fluid does not vary with the height, the third term is not taking into account into the explanation. Following these indications, the places where the airflow velocity is lower, have more pressure and vice versa.

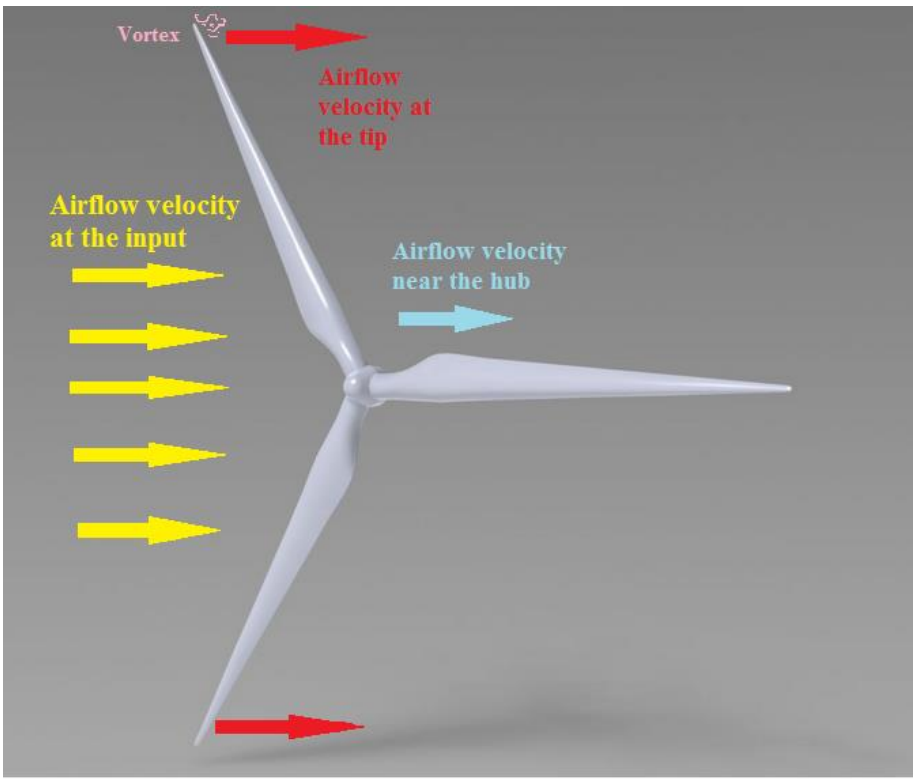

Figure 4.24: Airflow velocity

4.5.3. Pressure Contours

Essentially, the pressure contours over the wind turbines blades are seen in the Figures 4.25 and 4.26, below. As the name suggests, the leading edge of a blade is the part of the blade that first contacts air and for this reason. A greater differential is shown at the leading edge than the trailing edge, especially near the tip of the blade, where pressure gradient changes in a more violent way. It is mainly caused by the rotation effect. This pressure difference between the front and the back of the surface creates a lift force in the negative Z direction.

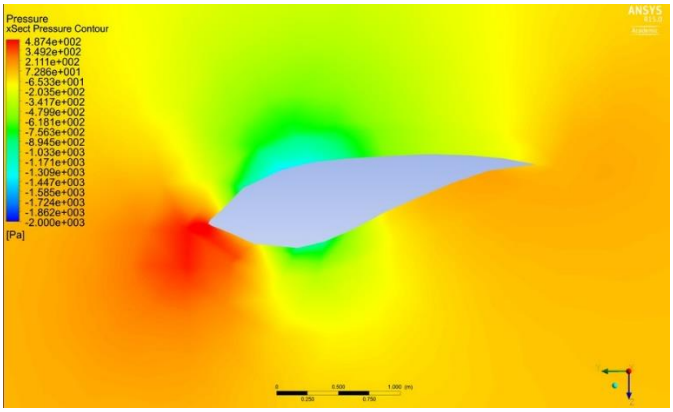

Figure 4.25: Pressure contours over the airfoil in ANSYS Fluent

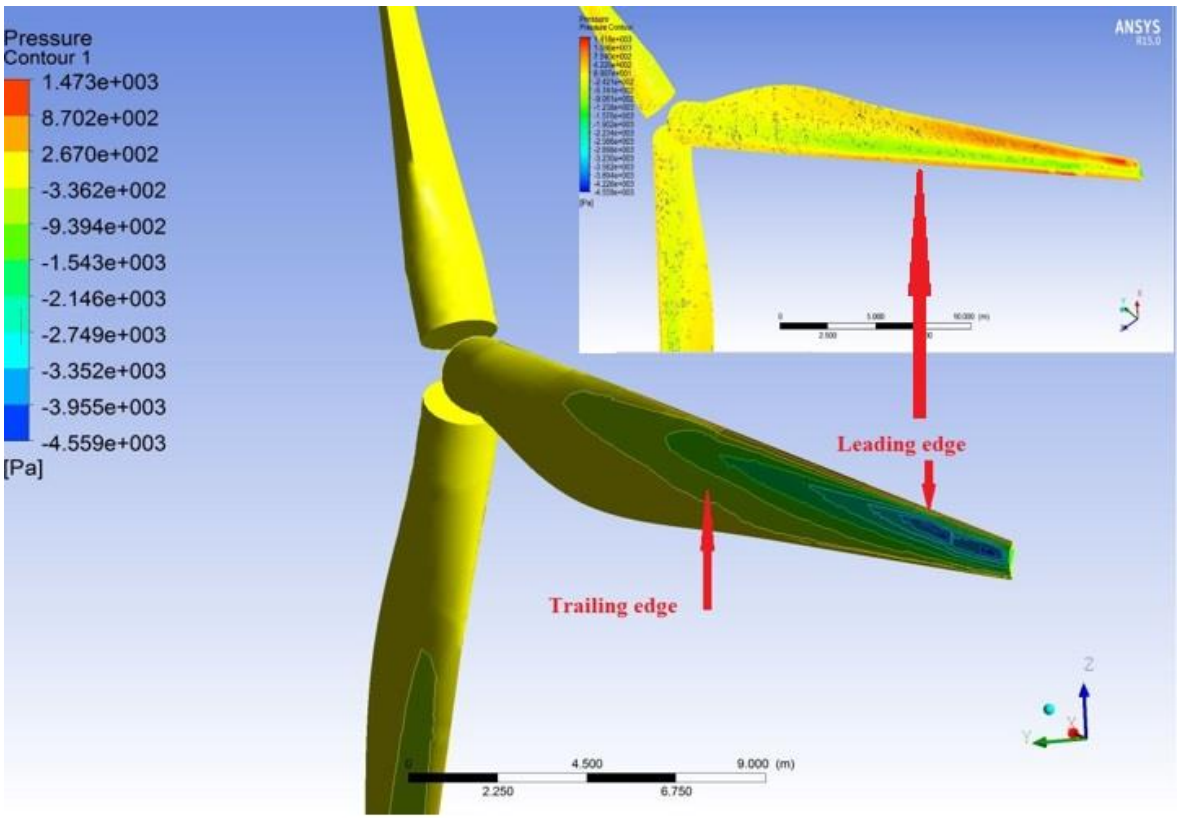

Figure 4.26: Pressure contours in ANSYS Fluent

4.5.4. Torque

Torque is a force that turns or rotates the wind turbine and it is equal to the force multiplied by distance. This means that so longer blades are, more torque can generate.

$$T = \frac{P}{\omega} = F \cdot x \quad (N \cdot m) \tag{4.9}$$

ANSYS provides a torque solution, as seen in Figure 4.27.

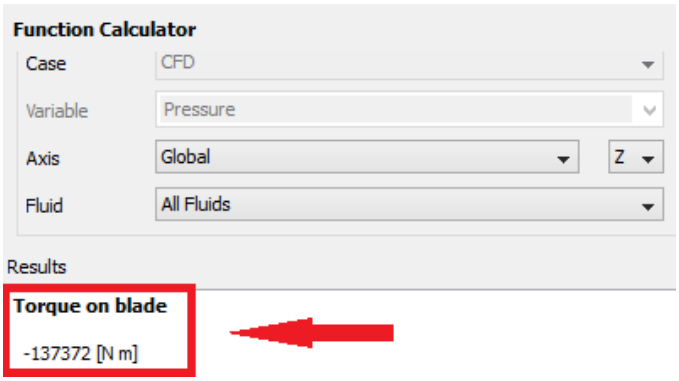

Figure 4.27: Torque on blade in ANSYS Fluent

4.5.5. Power coefficient

An estimate power coefficient value can be calculated by using the simple 1D Momentum Theory, [19]. This analysis incorporates some assumptions:

- The flow is steady, homogenous and incompressible.
- There is no frictional drag.
- There is an infinite number of blades.
- There is uniform thrust over the disc or rotor area.
- The wake is non-rotating.
- The static pressure far upstream and downstream of the rotor is equal to the undisturbed ambient pressure.

The power coefficient is defined as

$$C_p = \frac{P_{rated}}{P_{wind}} \tag{4.10}$$

According to the information presented in the problem specification section of this project, the blade follows the features of GE 1.5 XLE wind turbine blade. The specification sheet of this turbine states the rated power of this turbine to be 1.5 MW, the rated wind speed to be 11.5 m/s and the rotor diameter to be 82.5 m.
Plugging these data in the equation (4.10)

$$C_p = \frac{P_{rated}}{P_{wind}} = \frac{P_{rated}}{\frac{1}{2}\rho A V_{rated}^3} = \frac{1.5\ MW}{\frac{1}{2}\left(1.225\frac{kg}{m^3}\right)\left(\frac{\pi(82.5m)^2}{4}\right)\left(11.5\frac{m}{s}\right)^3} = 0.30 \tag{4.11}$$

ANSYS provides a mesh refinement study in order to evaluate the precision of the solution. A finer mesh can help achieve a more precise solution of the model but is more computationally expensive. Figure 4.28 demonstrates how the results change with a greater number of cells.

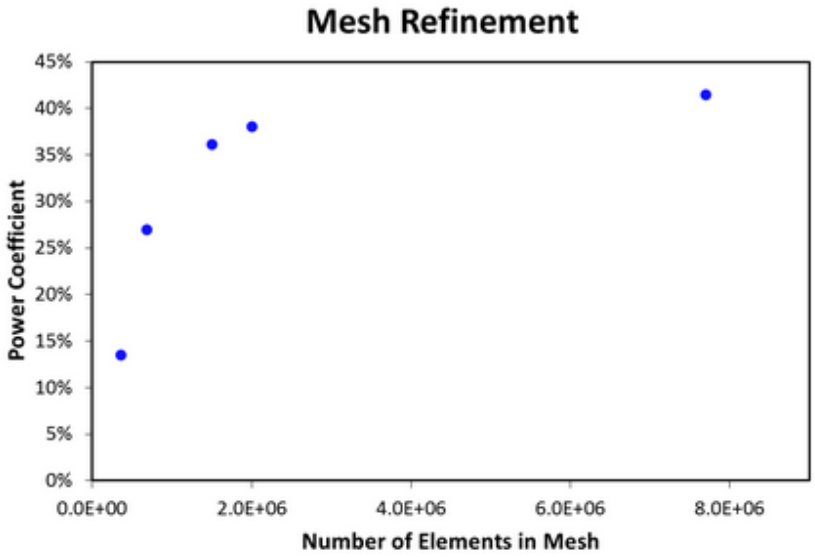

Figure 4.28: Mesh refinement study, [19]

The mesh created in the project has around 350,000 cells, so it is not fine enough to obtain an accurate solution. The C_p obtained in ANSYS is around 0.15, which indicates that the error between both studies is 15%. It is not a bad approximation in this case but future works might improve it.

Table 4.4: Power coefficient

Power coefficient:

Hand-calculation	CFD analysis	error (%)
0,30	0,15	50

An essential condition to verify is whether a sufficient number of iterations were performed in obtaining the solution is showed below. Figure 4.29 represents the solution behavior during the iterations. The number of iterations chosen is 3000 but the software stops the simulation before reaching to this number because the solution converged. The residuals do not change much between 1500 and 2135 iterations. This is why 1500 iterations was deemed appropriate, considering the reduction in solving time. 3000 iterations are solved in almost 6 hours whereas 1500 iterations are solved in 3 hours, it means the half time.

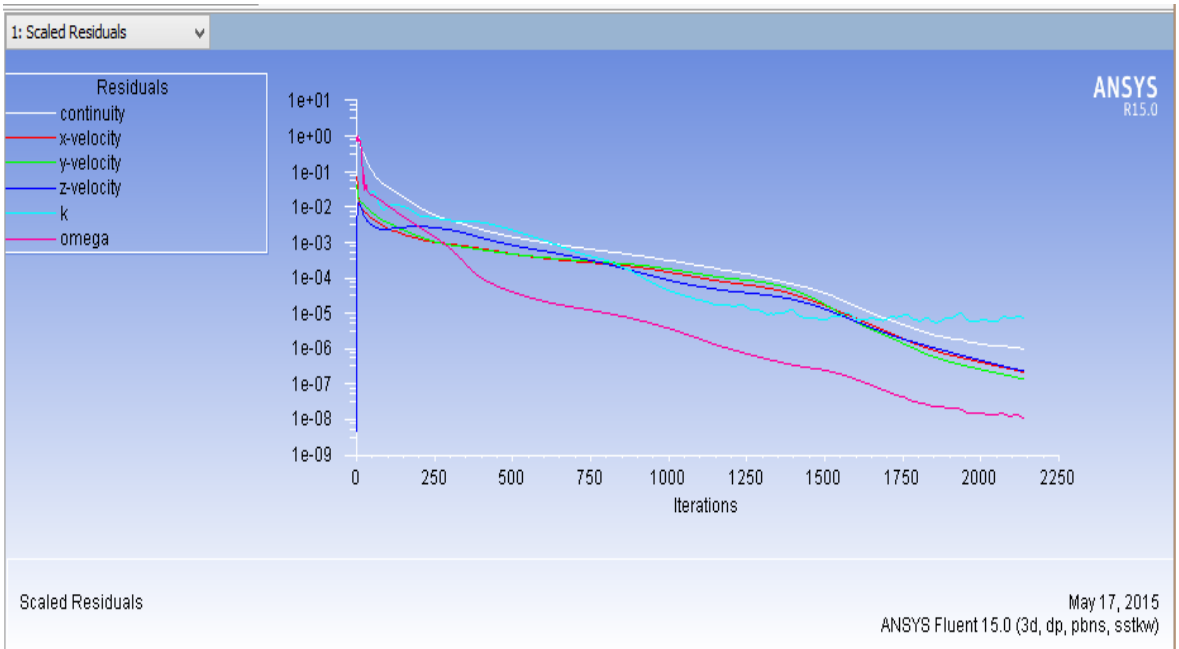


```
  2126  1.0441e-06  2.3408e-07  1.4778e-07  2.4825e-07  8.4022e-06  1.2540e-08 -7.6438e+04  1:30:08  874
  2127  1.0393e-06  2.3293e-07  1.4712e-07  2.4702e-07  8.3068e-06  1.2393e-08 -7.6438e+04  1:29:29  873
  2128  1.0339e-06  2.3179e-07  1.4641e-07  2.4580e-07  8.1845e-06  1.2263e-08 -7.6438e+04  1:28:57  872
  2129  1.0289e-06  2.3061e-07  1.4571e-07  2.4459e-07  8.0412e-06  1.2123e-08 -7.6438e+04  1:31:24  871
  2130  1.0240e-06  2.2942e-07  1.4505e-07  2.4337e-07  7.8807e-06  1.1993e-08 -7.6439e+04  1:30:26  870
  2131  1.0201e-06  2.2831e-07  1.4441e-07  2.4217e-07  7.7189e-06  1.1849e-08 -7.6439e+04  1:29:39  869
  2132  1.0152e-06  2.2723e-07  1.4380e-07  2.4096e-07  7.5615e-06  1.1723e-08 -7.6439e+04  1:29:00  868
  2133  1.0095e-06  2.2617e-07  1.4321e-07  2.3977e-07  7.4076e-06  1.1596e-08 -7.6439e+04  1:28:27  867
  2134  1.0025e-06  2.2491e-07  1.4264e-07  2.3859e-07  7.2566e-06  1.1496e-08 -7.6439e+04  1:28:00  866
  iter  continuity  x-velocity  y-velocity  z-velocity          k       omega  surf-mon-1     time/iter
! 2135 solution is converged
  2135  9.9650e-07  2.2377e-07  1.4207e-07  2.3741e-07  7.1074e-06  1.1390e-08 -7.6439e+04  1:27:37  865
Registering SurfaceMonitors, ("surf-mon-1.out")
```

Figure 4.29: Residuals study in ANSYS Fluent

Chapter 5

Structural Model of Wind Turbine

5.1. FSI (Fluid-Structure Interaction)

Fluid-structure interaction (FSI) describes the interaction between the solid structure (wind turbine blade) and a surrounding fluid flow (airflow). FSI is based on an interdisciplinary effort that conform meshes on both models (aerodynamic and structural) which allow to obtain analytical solutions in order to investigate the fundamental physics involved in the complex interaction between fluids and solids.

In this project, the performance of the wind turbine is a result of the interaction between airflow aerodynamics and structural model. Such an investigation is typically multidisciplinary and it remains a challenge due to their strong nonlinearity, thus the laboratory experiments are limited in scope in this field. Generally, FSI problems are developed using powerful software as ANSYS.

The software treats the fluid and the structure as two computational fields which are solved separately with their respective mesh discretization and equations. The boundary conditions of the domain and the whole geometry are used to connect both models, whereas the pressure solution of the aerodynamic part is imported into the structure model. Thus, it communicates information between the fluid and structure solutions, (see Figure 5.1).

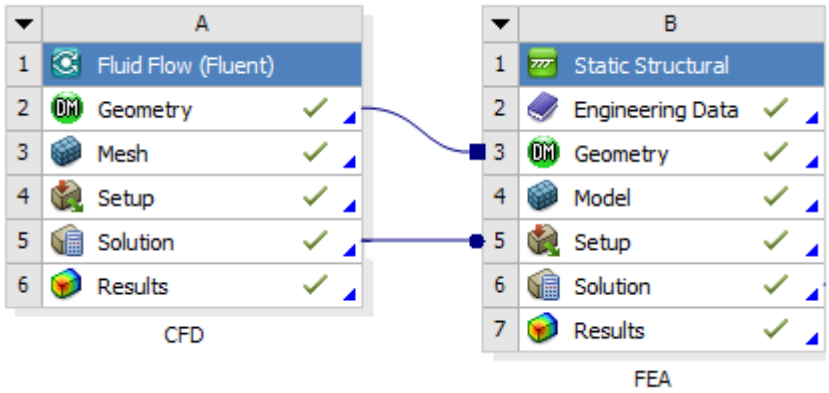

Figure 5.1: Fluid-Structure Interaction in ANSYS

5.2. Introduction

The structural design consists of blade material selection and the determination of stresses and deformations on wind turbine blades. The interaction between the flow and the blade concerns structural loads and deflections, which affect directly over the lifetime of the machine and it is also related with fatigue resistance.

It is evident that to satisfice objectives 3-6 detailed in page 37, the material must be selected carefully. The ideal material for blade construction will combine the necessary structural properties – namely high strength to weight ratio, fatigue life and stiffness – with low cost and the ability to be formed into the desired airfoil shape, [9].

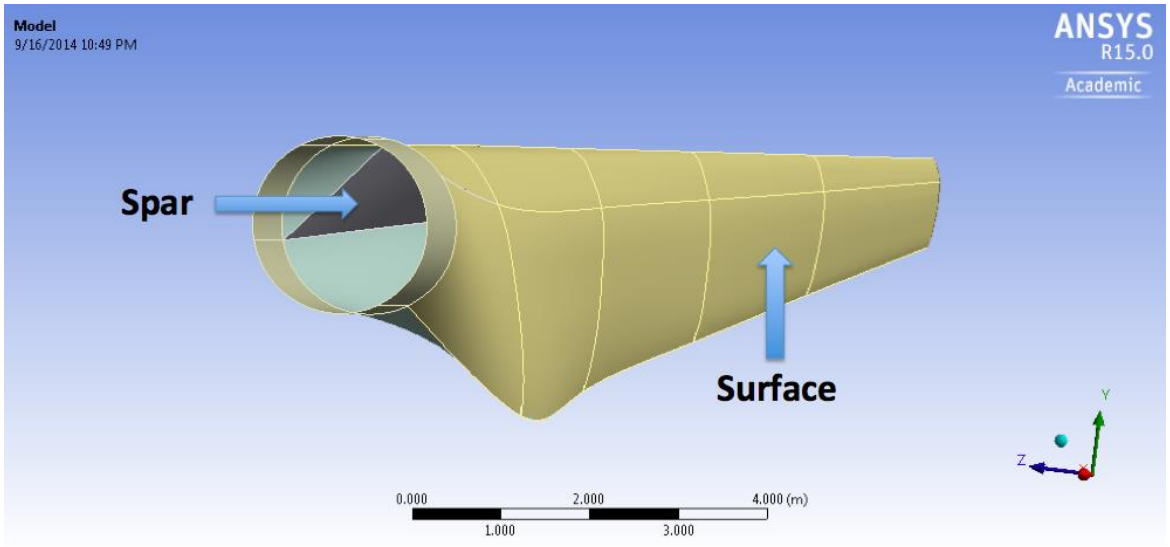

Figure 5.2: Blade in ANSYS Mechanical, [1]

As well as the aerodynamic design is based in the first part of the tutorial of the Cornell University web, structural model follows the steps of the second part of the same tutorial. In this case, the pressure load found using Fluent in part 1 is imported in Mechanical. The blade is composed of an outer surface and a structural cross section, commonly called spar (see Figure 5.2). It provides structural rigidity to withstand the loads. The thickness of the outside surface linearly decreases from 0.1 meters at the root to 0.005 meters at the tip whereas the spar has a similar thickness behavior with 0.1 meters at its closest point to the root and 0.03 meters at the tip, [19].

Table 5.1: Thickness specifications respect to the global coordinate system

Surface:		**Spar:**	
X (m)	**Thickness (m)**	**X (m)**	**Thickness (m)**
-1	0,1	-3	0,1
-44,2	0,005	-44,2	0,03

Static Structural is chosen in the *Analysis System Toolbox* of ANSYS and this analyses is called FEA (Finite Elements Analyze), as it is shown in Figure 5.3.

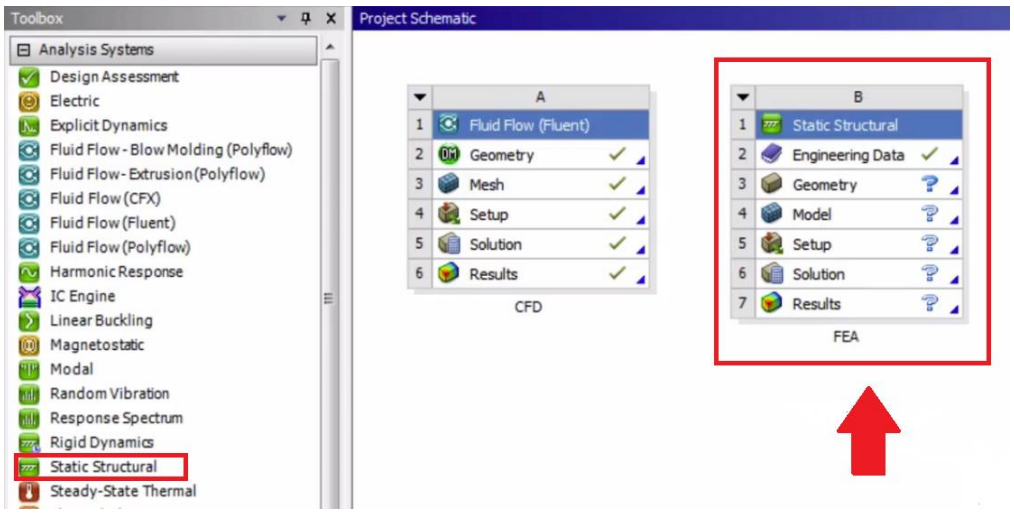

Figure 5.3: Initial screen from ANSYS Mechanical

5.3. Engineering Data

According to the material selection, wind turbine blades are made of composite materials in order to reduce the weight of the machine. Composite materials can be represented approximated by the following orthotropic material properties (see Figure 5.4).

Table 5.2: Orthotropic material properties, [19]

Material Properties:	
Density (kg/m^3)	1550
Young's Modulus-X (Pa)	1,1375E+11
Young's Modulus-Y (Pa)	7,583E+09
Young's Modulus-Z (Pa)	7,583E+09
Poisson´s Ratio-XY	0,32
Poisson´s Ratio-YZ	0,37
Poisson´s Ratio-XZ	0,35
Shear Modulus-XY (Pa)	5,446E+09
Shear Modulus-YZ (Pa)	2,96E+09
Shear Modulus-XZ (Pa)	2,96E+09

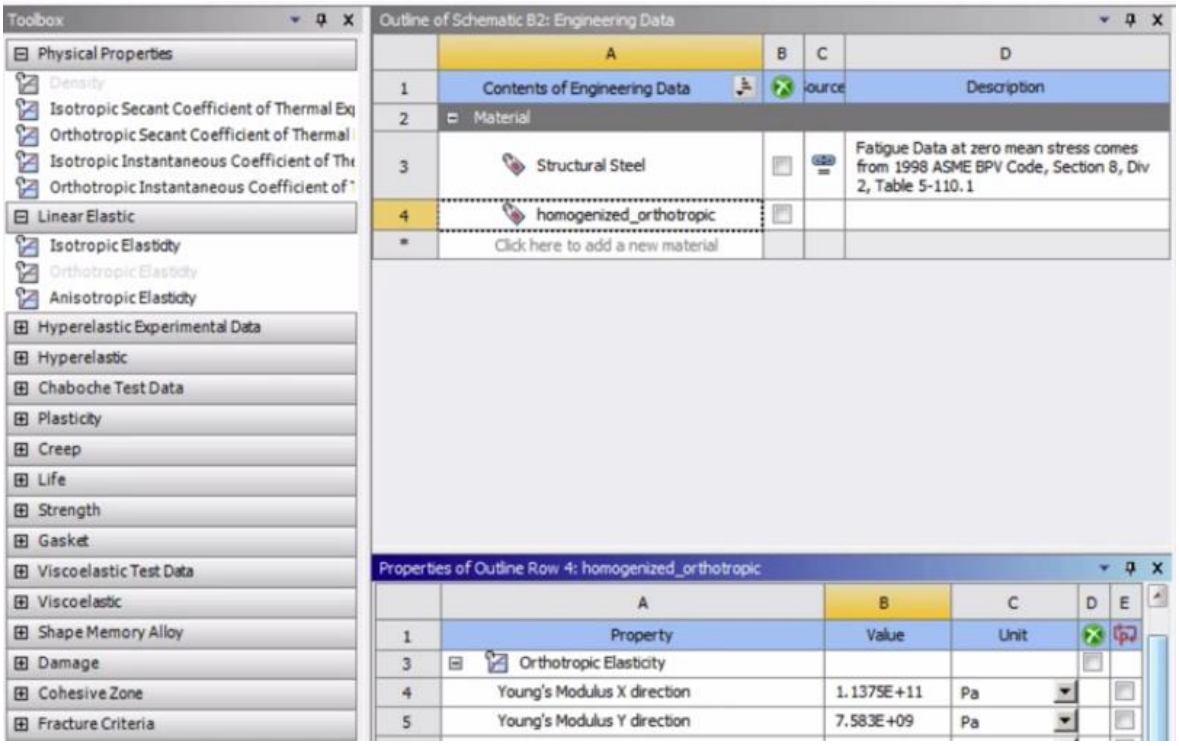

Figure 5.4: Orthotropic material properties in ANSYS Mechanical

5.4. Geometry

The blade geometry is imported by dragging the geometry cell from the CFD project to the geometry cell of the FEA project. Figure 5.5 describes graphically the connection between CFD project and FEA project due to the same blade geometry is used in both projects.

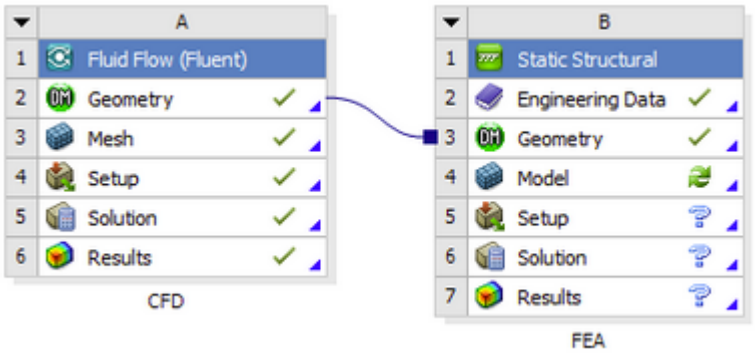

Figure 5.5: First connection between CFD project and FEA project, [19]

5.5. Model

This step consist of give the blade a proper mesh. In section 4.3 of the report, the mesh is chosen according *Fluent Physics Reference* and the cells have tetrahedral form whereas in this case, the mesh follows the *Mechanical Physics Reference* and the cells are quadrilateral elements as it is shown in Figure 5.6 and Figure 5.7. Quadrilateral cell shaped is a 4 sided one.

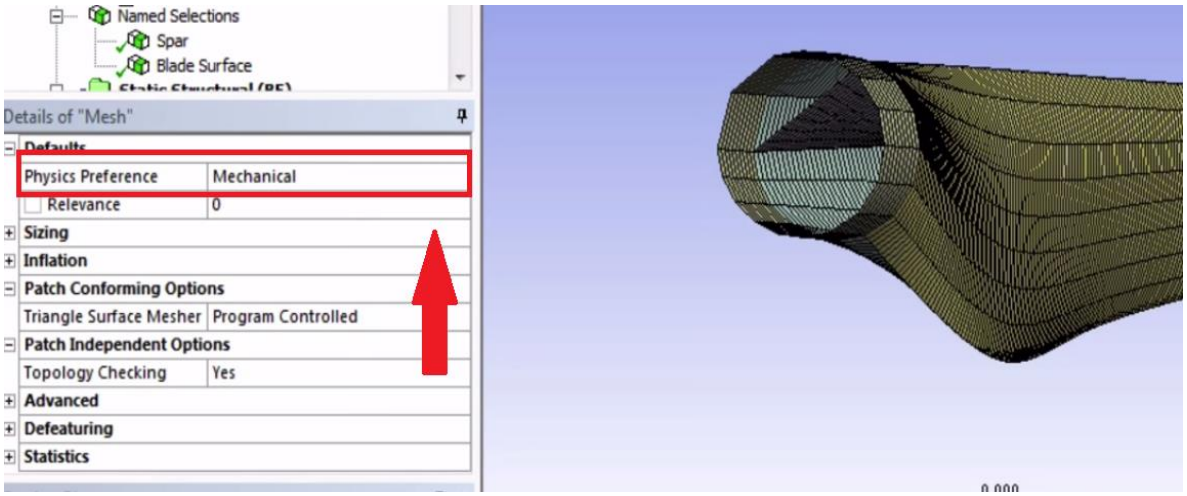

Figure 5.6: Mechanical Physics Reference

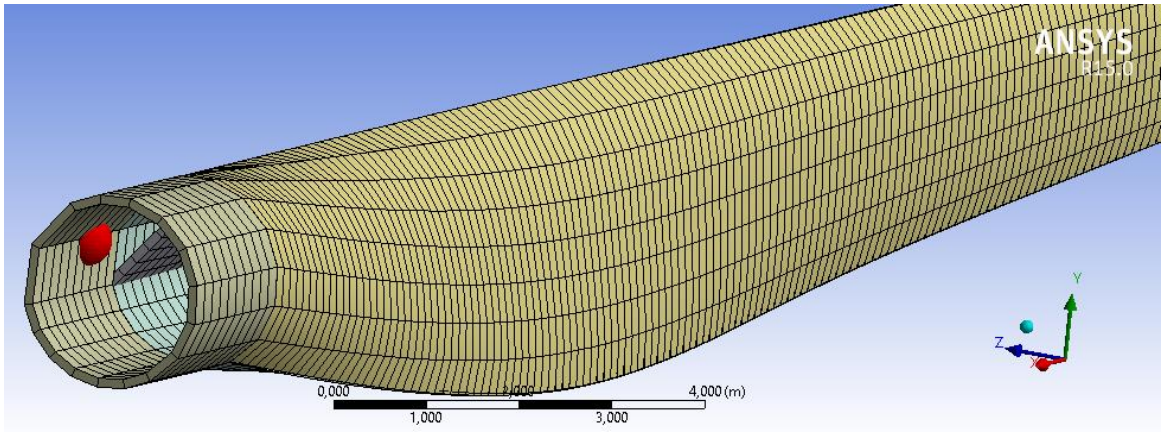

Figure 5.7: Structural Model mesh

The details of the mesh are represented in Figure 5.8. See that the total number of cells in the mesh of this structural design are around 3500 cells, an amount much lower than in the aerodynamic part. The mesh size is an important factor in determining the stability and accuracy of the methods and the number of cells are related to the complexity of the model and also with the number of equations needed.

Aerodynamic model involves complex wind turbine blade geometry and flow physics, in which smaller mesh size provides better approximation of the variables required. Due this, the mesh shaped cell chosen in the aerodynamic part is a tetrahedron, which is a 3D cell whereas it is used a quadrilateral cell in the structural model.

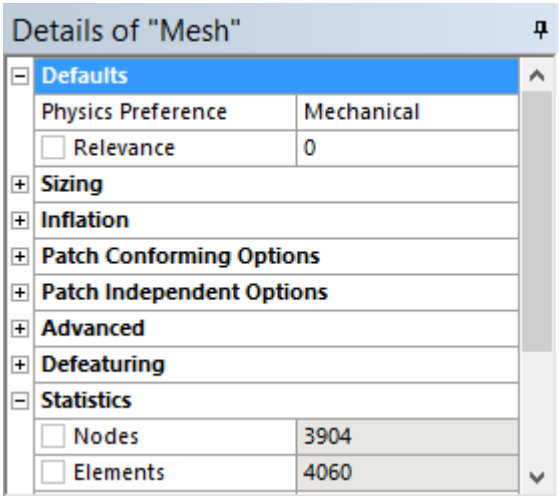

Figure 5.8: Details of the *Mesh* in ANSYS Mechanical

Two studies are used to judge the quality of the *Mesh*, whether it is a proper one. The skewness is very low and the orthogonal quality is very high, so as well as it is marked in Chapter 4, the mesh conforms to the requirements of both studies (see Figures 5.9 and 5.10).

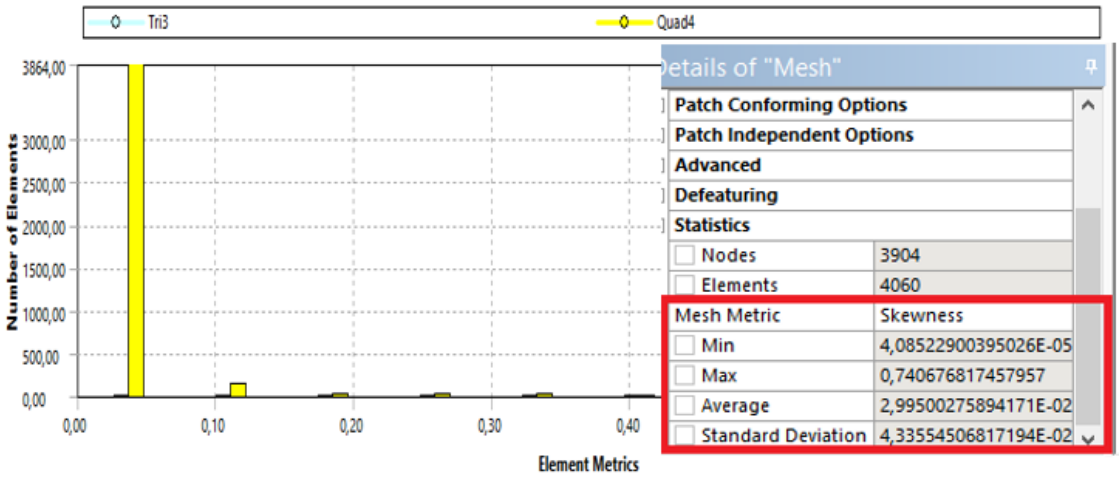

Figure 5.9: Skewness study in ANSYS Mechanical

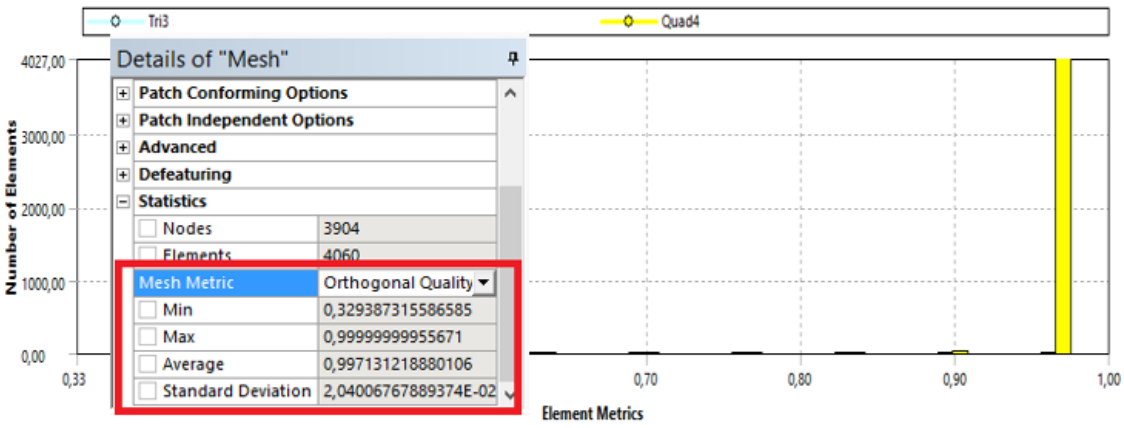

Figure 5.10: Orthogonal Quality in ANSYS Mechanical

5.6. Physics Setup

Once assigned the material, defined the thickness of the blade (the spar and the surface), and introduced the rotational velocity as $-2.22\ rad/s$ in the z-component, the pressures results from the CFD part are transferred into the FEA project by dragging the solution cell to the Setup cell, (see Figure 5.11).

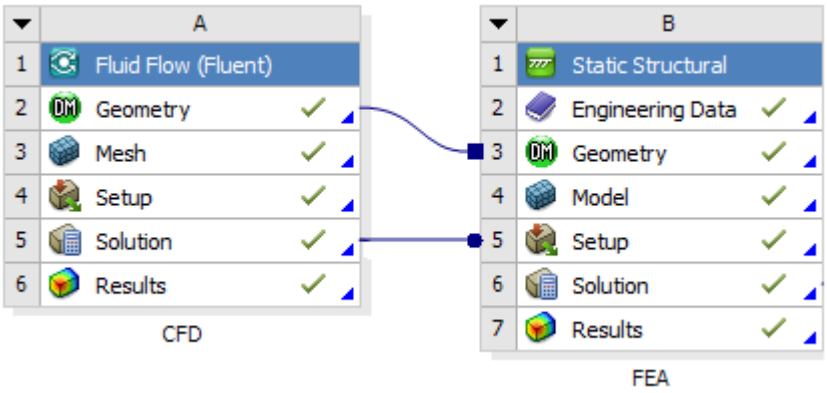

Figure 5.11: Second connection between CFD project and FEA project

5.7. Solution and Results

5.7.1. Total Deformation

The structural simulation provides several results. One of them is the total deformation of the wind turbine blade, as it is shown in the Figure 5.12. As it was expected, the maximum deformation occurs at the blade tip whereas the deformation of the blade near the hub is almost insignificant. The maximum tip displacement is **0.47392 meters**.

This deformation distribution is because of the tip suffers high loadings related with the rotation and the velocity of the airflow. Figure 5.13 illustrates the deflection of the wind turbine blade.

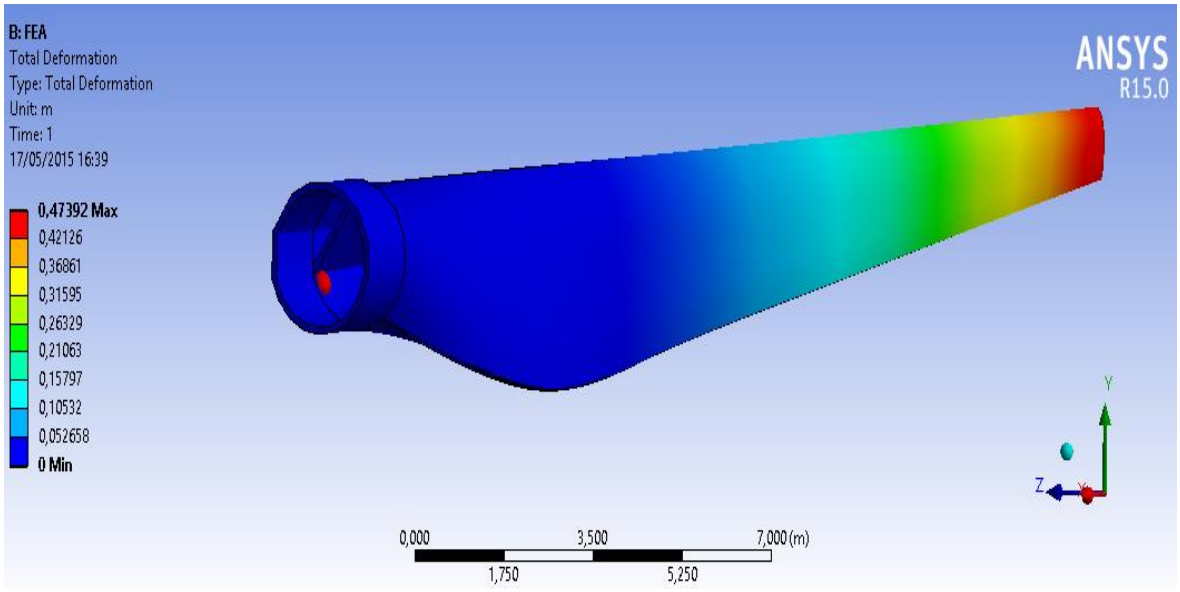

Figure 5.12: Total deformation of the blade in ANSYS Mechanical

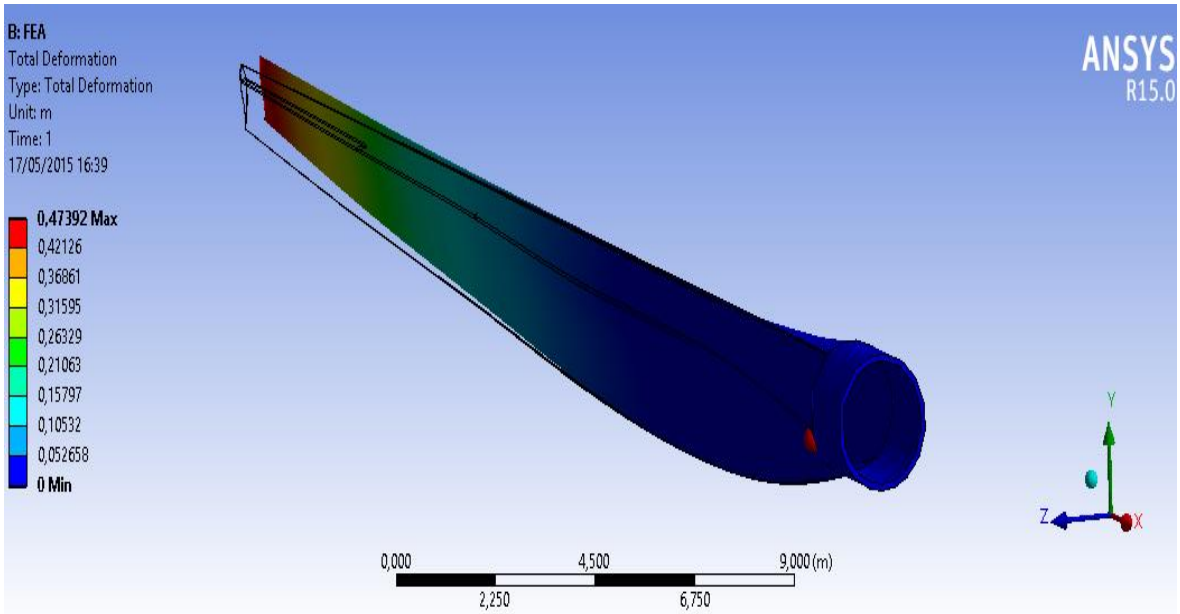

Figure 5.13: Deflection of the blade in ANSYS Mechanical

5.7.2. Equivalent Stress

It is important to show and detect where the maximum stresses occurs. ANSYS provides a stress distribution of the blade and it shows that the stress at the trailing edge of the wind turbine blade is smaller than in the leading edge, (see Figure 5.14).

In this model, the max Von-Mises stresses appear, after the vibration of the HAWT blade because of the passing wind. Due to the loads at the tip, max Von-Mises stresses reaches the maximum, and it is mainly concentrated in the central part of the blade (closer to the tip than the hub part), as it is observed in Figure 5.15. Due the high stress, this part of the blade is weaker.

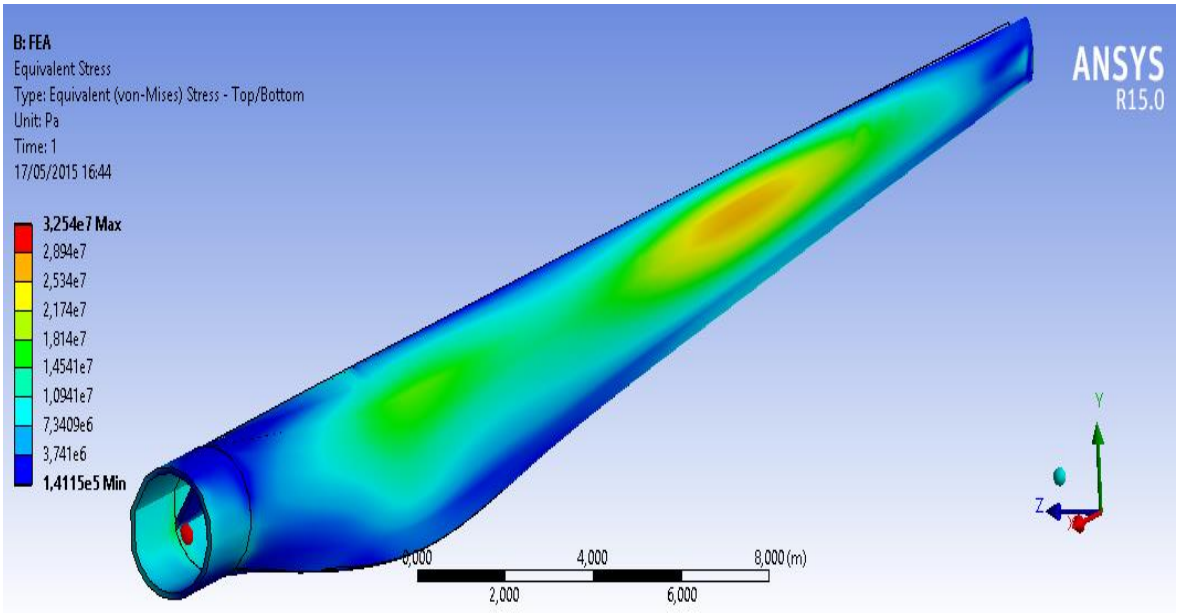

Figure 5.14: Stresses on the blade in ANSYS Mechanical

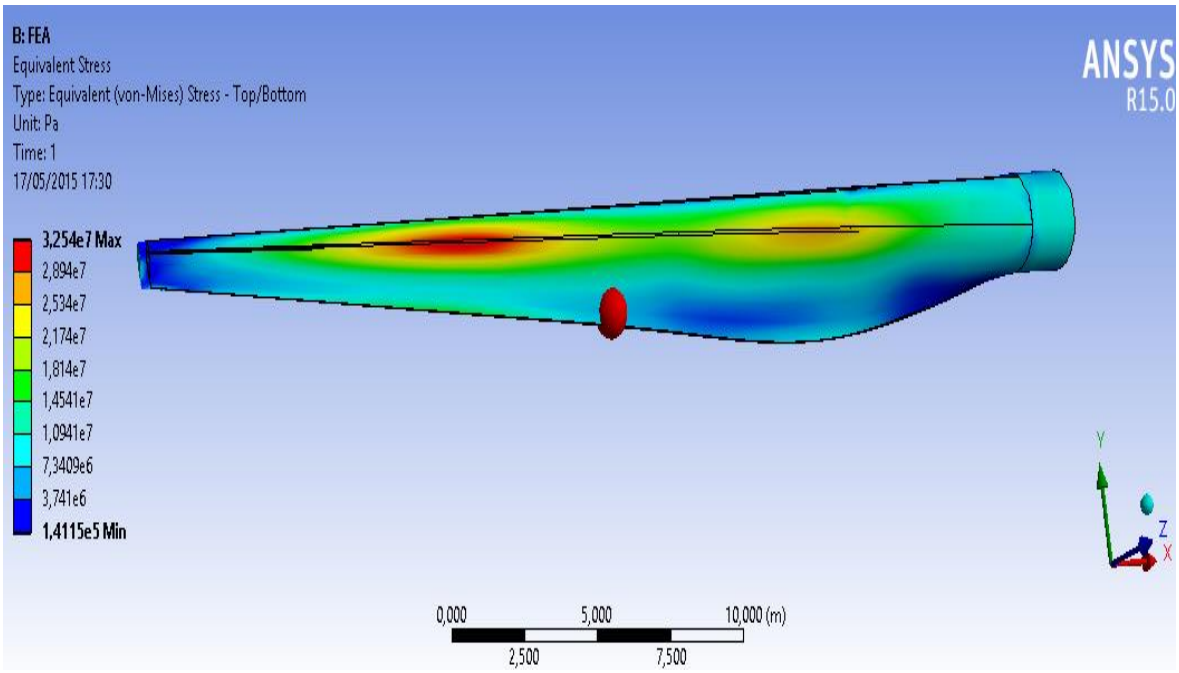

Figure 5.15: Maximum stress on the blade in ANSYS Mechanical

5.7.3. Force Reaction

First of all, a hand-calculation is done based on the classical dynamic theory in order to find the root radial force, which is the outward force that comes from the mass. Note that it is equal in value and opposite according to the direction of to the reaction force at the root of the blade that keeps the blade connected to the hub. The radial force of the wind turbine blade follows the equation below

$$F_{radial} = -mr\omega^2 \tag{5.1}$$

Taking into account the data specified by the software about the characteristics of the wind turbine blade, it weighs 22473 kg and its center of mass in the coordinates (X, Y, and Z) follows the (-14.232 m, -0.2127 m, 0.15969 m) localization, (see Figure 5.16). Plugging these values in the equation (5.1), the radial force is 1465.5 KN.

```
***********  PRECISE MASS SUMMARY  ***********

TOTAL RIGID BODY MASS MATRIX ABOUT ORIGIN
            Translational mass                |   Coupled translational/rotational mass
      22473.        0.0000        0.0000      |     0.0000        3588.7        4780.0
      0.0000        22473.        0.0000      |    -3588.7        0.0000      -0.31985E+06
      0.0000        0.0000        22473.      |    -4780.0       0.31985E+06    0.0000
  ----------------------------------------- | -----------------------------------------
                                              |         Rotational mass (inertia)
                                              |     19493.       -64350.        85538.
                                              |    -64350.       0.65791E+07   -2717.2
                                              |     85538.       -2717.2       0.65874E+07

TOTAL MASS =  22473.
  The mass principal axes coincide with the global Cartesian axes

CENTER OF MASS (X,Y,Z)=   -14.232      -0.21270       0.15969
```

Figure 5.16: Characteristics of the mass in ANSYS Mechanical

This data is compared with the value of the radial force obtained by ANSYS, which is showed in the Figure 5.17. The error obtained is 7.8%, so it is considered a good approximation.

Details of "Force Reaction"	
Result Selection	All
Display Time	End Time
Results	
Maximum Value Over Time	
X Axis	1,5781e+006 N
Y Axis	15255 N
Z Axis	72058 N
Total	1,5798e+006 N
Minimum Value Over Time	
X Axis	1,5781e+006 N
Y Axis	15255 N
Z Axis	72058 N
Total	1,5798e+006 N
Information	

Figure 5.17: Force reaction in ANSYS Mechanical

Table 5.3: Radial Force

Radial Force:

Hand-calculation (KN)	CFD analysis (KN)	error (%)
1465,50	1579,8	7.8

5.7.4. Moment Reaction

The moment reaction is given by ANSYS in the Figure 5.18. It is $2515.2\ KN \cdot m$ and as it was expected, the majority of the reaction is in Y-axis because of the features of the model.

Schematically, the geometry of the blade is developed in X-direction, so when the wind reaches the blade in Z-direction, the blade suffers a radial force in the direction of the blade. Besides, the airflow applies a force on the blade which implies a moment reaction in Y-direction and also it means a rotational movement of the wind turbines blades.

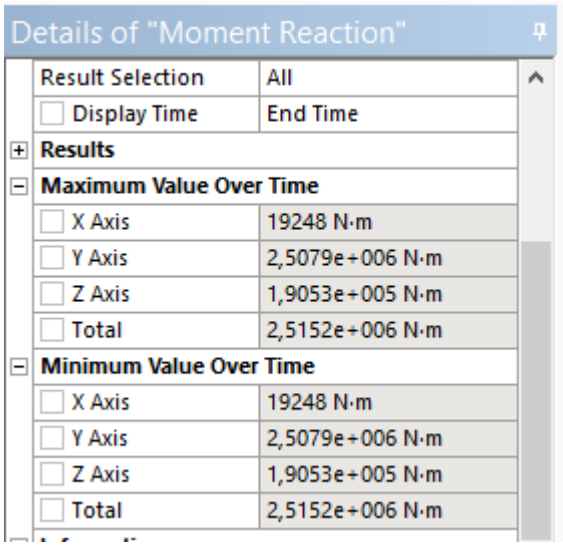

Figure 5.18: Moment reaction in ANSYS Mechanical

5.7.5. Total Displacement

Figures 5.19 and 5.20 show the total displacement of the wind turbine blade after importing the pressure from the aerodynamic model. All around the blade are arrows which are used to illustrate the imported pressure vectors in the surface and how the displacement takes place. Note that at the tip of the blade, the color of the vectors is red, which means that on this part the higher pressure is concentrated.

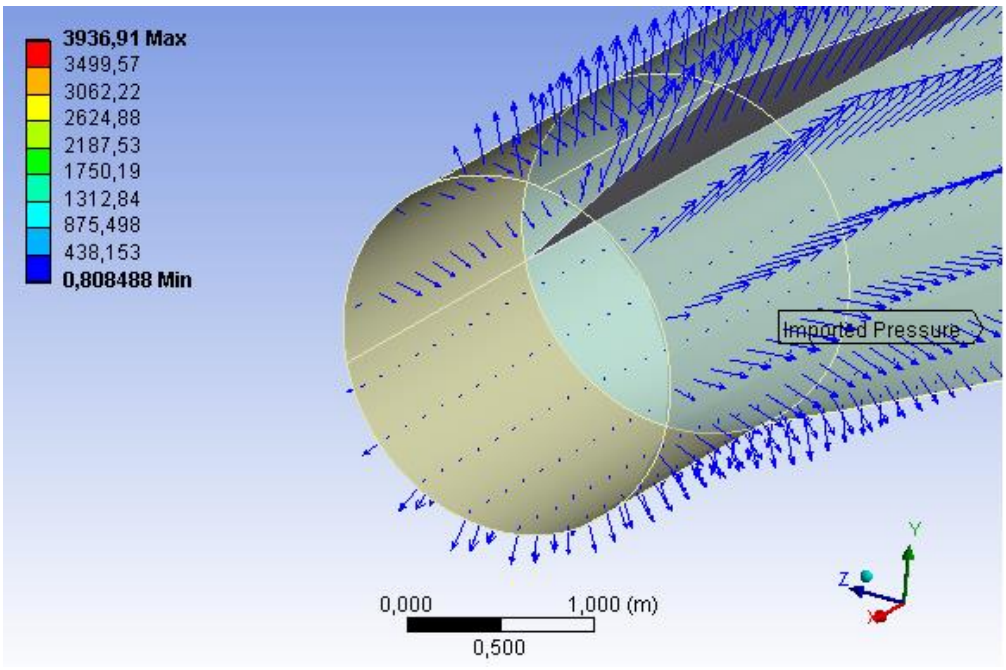

Figure 5.19: Imported pressure over the wind turbine blade

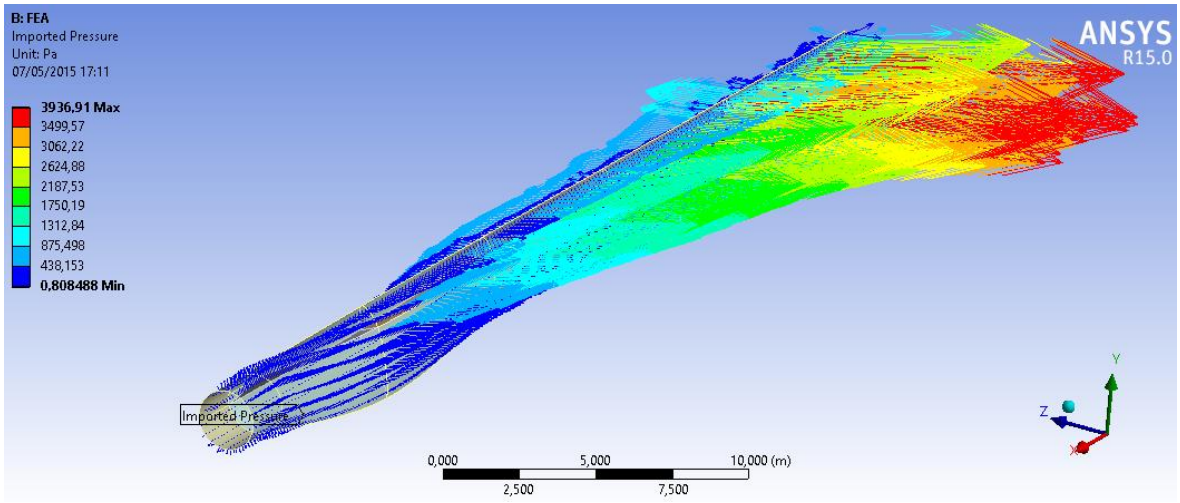

Figure 5.20: Wind turbine blade deformation

Conclusions

This master thesis studies the dynamics of horizontal wind turbine blades taking into account the aerodynamic behavior and the elasticity of rotor blades, also the steadiness of flow. The research of aerodynamic and dynamic behavior of HAWT blades, combined with reporting on the elasticity of its construction by using the one solver, is a labor-intensive task. The difficulty comes from the inability to simultaneously solve the equations of fluid mechanics, describing the flow, and structural dynamics. Therefore, it is been used numerical approach using both numerical models that is been developed with the help of ANSYS software.

In order to calculate the aerodynamic loading of HAWT blades, there it is been developed an aerodynamic model for studying of the flow around HAWT rotor, which employs the Finite Element Method (FEM) and FLUENT solver. In the aerodynamic model, first the blade geometry is imported from Solid Work, another CAD program that is used to design in advance the geometry of one wind turbine blade, after that using the tools of ANSYS software the other two blades from the HAWT is designed, and it is model the fluid domain. After created the proper fluid domain, a mesh is created around the blades and the Fluent solver is then used to find aerodynamic loading on the blades, also to consider the fluid flow field. To consider the elasticity of the HAWT blades it is developed second numerical model called structural model realized again through ANSYS software but using the ANSYS mechanical. The pressure of the wetted areas of the blades that is took it from the aerodynamic solver are imposed as the pressure loads to the Structural model to determine the stresses and deformations on the HAWT blade. The main value of that project is that here it is considers the deformations of the HAWT blade due to the aerodynamic loading of the wind turbine blade by performing a steady-state FSI (Fluid-Structural Interaction) analysis.

The validation of the obtained numerical results with developed aerodynamic model is been performed by verification of the corrected numerical simulation realized through the sufficient number of iterations for obtaining the pressure on the blade that has converged pointed out into the Chapter 4 Aerodynamic Model of Wind Turbine. The figure of iteration process that is given in Chapter 4 illustrating the solution convergence, and information that is given on the figure that residuals from the iterative process do not change much between 1500 and 2135 iterations. Hence, the last statement is a prerequisite to accept that 1500 iterations is sufficient number of iterations to obtained relative good convergence of the numerical solution into the simulations realized with developed aerodynamic model. Therefore, the approximately good convergence of the aerodynamic solver is a prerequisite to confirm that the obtained results for aerodynamic loading over the HAWT blade is approximately good.

The last statement is verified with the tools of mesh refinement into the aerodynamic solver, and the fact that mesh size number of around 356 314 cells is a fine enough to obtained the sufficiently accurate results for the purpose of that project. The sufficient number of mesh size used for the aerodynamic model is confirmed by the relatively good correspondence of the obtained numerical results for the cp power coefficient 15% compared of those result made by hand calculations 30% using the 1D Momentum Theory, and explained in Chapter 4.

The validation and verification of the developed Structural model used for determination of the HAWT blade deformation due to the aerodynamic loading of a wind turbine blade by performing FSI analysis is made by comparison of the numerical results of root radial force with those obtained by the hand-calculation. The approximately good correspondence from 7.8% obtained for the root radial force F_{radial} of the wind turbine blade between the obtained numerical results and those from the hand calculation are the prerequisite to confirm validation of the developed Structural model using for determination of the stresses and deformations of the wind turbine blades.

Of course both numerical models used to fulfil the purpose of that project have its disadvantages as:

- Aerodynamic solver used for calculation of the aerodynamic loading of HAWT blades is developed in case when the flow field is incompressible. But the actual flow field around the HAWT is compressible and in this can be pointed as the next step or tendency of further development of that model.

- Also there are no experimental results that can be used to validate the numerical results obtained with both numerical models. Therefore, it is worth to mention that if the idea underlying into this project is expand in bigger investigation into that area it can be made the experimental part and obtained sufficient number of experimental data using to confirm those obtained by numerical simulations.

- The developed Structural model does not have sufficient number of cell for the mesh using into the simulations. But it is worth to mention that for this state of that study it is not necessary to have so big accuracy into the mechanical part of that project. But again as a recommendation it can be consider the opportunity the structural model to be performed to the other types of wind turbine blades with different physical properties and also to have more precision into the results to use the tool of mesh refinement into the Mechanical part.

The realize study into this project and the obtained relative good correspondence between the obtained numerical results and those from hand calculation for both numerical models: aerodynamic and structural are the conformation that developed both model work and it can be used in the preliminary stage of design of HAWT blades. In order to investigate in details the complex flow field around HAWT blade, it is advisable for the next stage of that project to be considering the unsteadiness of flow close to the real one.

References

[1] Alberto Mazzoldi. Leakage and atmospheric dispersion of CO2 associated with carbon capture and storage projects (thesis). *University of Nottingham*, March 2009.

[2] Renewables 2014, Global Status Report. REN21 Renewable Energy Policy Network for the 21st Century. www.ren21.net

[3] Renewable energy technologies: cost analysis series. Volume 1: Wind Power. *IRENA International Renewable Energy Agency*. June 2012.

[4] Martin O.L. Hansen. Aerodynamics of Wind Turbines. Second edition, 2008.

[5] Damien Robinet. Les energies renouvelables. December, 2014

[6] Funes Ruiz, J. Análisis simplificado de la respuesta estructural de una pala de aerogenerador (thesis). July 2009

[7] Joseba Ripa. Wind turbines aerodynamics and wind characteristics. *Energy Technology of Public University of Navarre*. 2013

[8] Spera, D. Wind turbine technology. Fundamental concepts of wind turbine engineering. *The American Society of Mechanical Engineers*, 1995.

[9] Burton, T.; Sharpe, D.; Jenkins, N; Bossanyi, E. Wind Energy Handbook. *John Wiley & Sons*, Chichester, UK, 2001.

[10] Eric Hovanitz. Global circulation. *Santiago Canyon College*. 2014.

[11] Wind turbines. Mechanical Engineering. Boston University.

[12] Magdi Ragheb and Adam M. Ragheb. Wind Turbines Theory - The Betz Equation and Optimal Rotor Tip Speed Ratio. *Department of Nuclear, Plasma and Radiological Engineering and Department of Aerospace Engineering.* USA.

[13] National Aeronautics and Space Administration. http://www.grc.nasa.gov/

[14] Environmental Green Science. Wind Power. www.environmental/green-science/wind-power3.com

[15] J. D. Anderson, Introduction to Flight, McGraw-Hill, ISBN 0-07-282569-3, 2004

[16] Computational fluid dynamics of wind turbine blade at various angles of attack and low Reynolds number. S.Rajakumar. International Journal of Engineering Science and Technology. Vol.2. 2010, 6474-6484.

[17] Smart Blade Company. www.smart-blade.com

[18] S. Santoso and H. T. Le, *"Fundamental time-domain wind turbine models for wind power studies,"* Renewable Energy, vol. 32, no. 14, pp. 2436–2452, 2007.

[19] Cornell University. MAE 4021 Project Guide Rev. 10/29/2013

[20] NREL/SR-500-36343 D.M. Somers *Airfoils, Inc. State College, Pennsylvania*. The S827 and S828 Airfoils Period of Performance: 1994 – 1995.

[21] ANSYS, Theory reference, 2007.